



The Sustained Global Ocean Observing System For Climate

FY 2008

ANNUAL REPORT

CLIMATE OBSERVATION DIVISION
NOAA CLIMATE PROGRAM OFFICE

NOAA, National Oceanic and Atmospheric Administration
www.noaa.gov

NOAA Climate Observation Division
www.oco.noaa.gov

Chapter II

The Global Oceans chapter is extracted from the "State of the Climate for 2008" report (Peterson, T. C., and M. O. Baringer, Eds., 2009: State of the Climate in 2008. Bull. Amer. Meteor. Soc., 90, S1-S196) and is reprinted courtesy of the American Meteorological Society.

This chapter should be cited as follows: Levy, J. M., Ed., 2009: Global oceans [in "State of the Climate in 2008"]. Bull. Amer. Meteor. Soc., 90, S1-S196.

3. GLOBAL OCEANS—J. M. Levy, Ed.

a. Overview—J. M. Levy

As the global ocean observing system matures and climatologies of essential climate variables grow more robust, observations of anomalous departures continue to shed light on the evolving behavior of the coupled ocean–atmosphere system. 2008 was characterized by the following findings.

The global mean SST in 2008 was slightly cooler than that in 2007, largely due to the cooling in the central tropical Pacific, the Arctic Ocean, and the regions extending from the Gulf of Alaska to the west coast of North America. The yearly mean SST anomaly in 2008 was dominated by a negative PDO pattern. The yearly mean PDO index in 2008 was the lowest since 1971.

Global integrals of upper-ocean heat content for the last several years have reached values consistently higher than for all prior times in the record, demonstrating the dominant role of the oceans in the Earth's heat budget. 2008 basin-scale upper-ocean heat content patterns are consistent with current phasing of familiar climate indices such as ENSO.

The basin-averaged latent and sensible heat fluxes in 2008 decreased slightly from 2007, continuing the broad downward trend that started in 1999. There seems to be a tendency toward reversing the upward trend that had dominated the decades of the 1980s and 1990s. Changes in latent and sensible heat fluxes in the Pacific responded to the SST anomalies of the cool PDO phase, with enhanced heat loss over positive SST anomalies and reduced heat loss over negative SST anomalies. By contrast, the ocean heat fluxes in the Atlantic Ocean were an important forcing for SST variability: SST increased as a result of reduced heat loss at the sea surface and decreased as a result of enhanced heat loss at the surface.

Tropical cyclone heat potential values in the north-central Gulf of Mexico were lower in August 2008 than in August 2005.

Outside the tropics, the anomalously salty surface salinity values in climatologically drier locations and anomalously fresh values in rainier locations observed in recent years generally persisted in 2008, suggesting an increase in the hydrological cycle, consistent with climate model predictions for global warming scenarios. Within the tropics, 2008 sea surface salinity anomalies can be largely related to recent La Niña conditions.

Eastward surface current anomalies in the tropical Pacific Ocean in early 2008 played a major role in adjusting the basin from strong La Niña conditions to ENSO-neutral conditions by July–August. Long-term

trends in geostrophic eddy kinetic energy continue to indicate interannual-to-decadal shifts in major current systems such as the Gulf Stream and the Brazil–Malvinas Confluence.

Direct observations of the strength of the meridional overturning circulation show substantial variability on short time scales, with some evolving evidence of a pronounced seasonal variation. Indirect observations from subsurface water properties suggest a recent strengthening of deep-water formation in the Labrador Sea and a decrease in deep-water transport from the Antarctic that is both warmer and fresher than in the past.

The La Niña event of 2007–08 affected not only regional sea level anomalies but GMSL as well. GMSL has been persistently low during the La Niña event relative to a linear trend of approximately 3.3 mm yr^{-1} . The correspondence between GMSL and the Multivariate ENSO Index highlights the strong influence of ENSO variability on global sea level. Once this interannual variability is accounted for, the inferred rate of GMSL change remains remarkably constant.

The global mean air–sea CO_2 flux for the period 1983 to 2007, including ENSO effects, gives an average uptake of $1.74 \text{ Pg-C yr}^{-1}$. The global mean CO_2 uptake for 2007 is estimated to be 1.67 Pg-C , about 0.07 Pg-C lower than the long-term average, making it the third-largest anomaly determined since 1983. Unlike long-term findings, the North Atlantic has not had the largest increase in anthropogenic carbon storage over the last decade. The rate of carbon inventory increase in the eastern Indian Ocean was significantly higher between 1995 and 2008 than it was between 1978 and 1995.

Global phytoplankton chlorophyll concentrations were slightly elevated in 2008 relative to 2007, but regional changes were substantial (ranging to about 50%) and followed long-term patterns of net decreases in chlorophyll with increasing sea surface temperature.

b. Sea surface temperatures in 2008—Y. Xue and R. W. Reynolds

The global SSTs in 2008 were analyzed using the OISST v.2, which is a weekly analysis on a 1° grid derived by combining *in situ* and satellite observations for the period of November 1981 to present (Reynolds et al. 2002). To put the 2008 SST in a historical perspective, we also analyzed the ERSST v.3b, which is a monthly merged land–ocean surface temperature analysis on a 2° grid for the period of 1854 to present (Smith et al. 2008). SSTA were

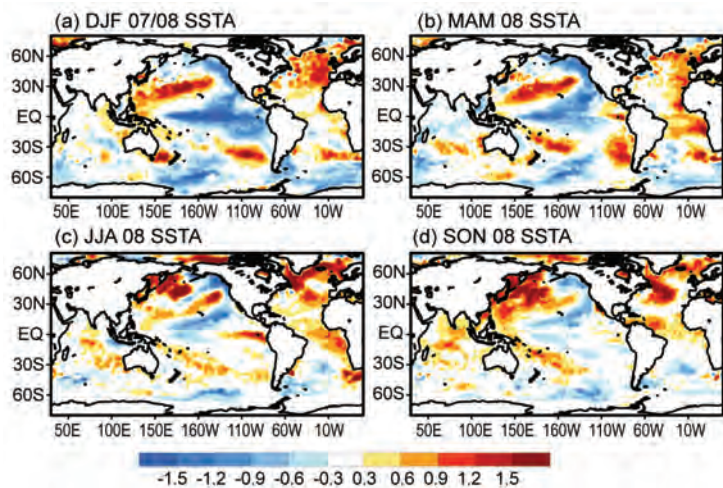


FIG. 3.1. Seasonal mean SST anomalies (°C) for (a) Dec 2007 to Feb 2008, (b) Mar to May 2008, (c) Jun to Aug 2008, and (d) Sep to Nov 2008. SSTs are the monthly fields interpolated from the weekly 1° OI analyses of Reynolds et al. (2002). All anomalies are defined as departures from the 1971–2000 climatology (Xue et al. 2003).

defined as departures from the 1971–2000 climatology described by Xue et al. (2003).

The seasonal evolution of SSTAs in 2008 is shown in Fig. 3.1. The SSTAs were generally positive in the Atlantic. In the Pacific basin, SSTAs were negative in the tropics related to the termination of a moderate La Niña. The 2007–08 La Niña started in August 2007, reached its mature phase during December 2007 to February 2008, and then dissipated quickly with the return of ENSO-neutral conditions in June 2008. La Niña conditions, however, reemerged during November 2008 to January 2009 (see NOAA’s ENSO definition at www.cpc.ncep.noaa.gov/products/analysis_monitoring/ensostuff/ensoyears.shtml). Both the demise and the reemergence of La Niña lagged associated surface current anomalies (see Fig. 3.14 and accompanying discussion).

During the first half of 2008, strong negative anomalies were present off the west coast of North America, while positive anomalies occurred along a rough sideways “V” pattern connecting the far western equatorial Pacific to 160°W at both 30°N and 30°S. Strong positive anomalies were also present north of 30°N in the Atlantic and western Pacific. These northern positive anomalies were strongest between July and October, with associated positive anomalies in the Arctic Ocean between the date line and 120°W. The Arctic Ocean SST was above normal in 2008, but it was about 1.3°C lower than its historical high of 2.5°C observed in 2007 (not shown). Consistently, the sea-ice extent in 2008 was larger than its

historical low in 2007 (<http://nsidc.org/arcticseaicenews/index.html>).

In the North Atlantic, SST has been persistently above normal since 1995. In the tropical North Atlantic, SST was near normal in the first half of 2008 but increased to about 0.6°C above normal during the Atlantic hurricane season from June to November (see details in the Tropical Cyclones section of chapter 4 of this report). In the eastern tropical Atlantic, SST has been persistently above normal during the past three years.

The yearly mean SSTA in 2008 was dominated by a negative PDO pattern (Mantua et al. 1997), which featured below-normal SST near the Gulf of Alaska and along the west coast of North America and above-normal SST in the central North Pacific (Fig. 3.2a). (The PDO spatial pattern and associated temporal PDO index are defined at <http://jisao.washington.edu/pdo/>.) Monthly and annual time series of the PDO index are shown in Fig. 3.3. The negative PDO phase began in September 2007 and

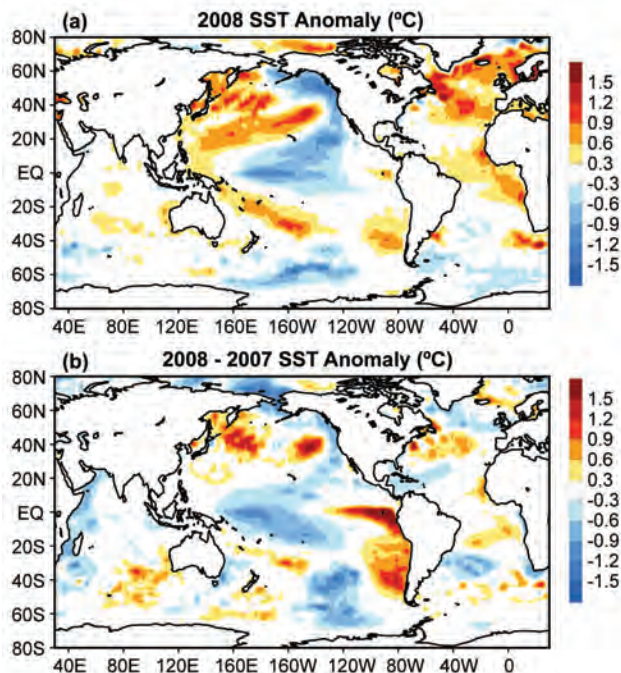


FIG. 3.2. (a) Yearly mean SSTA in 2008 and (b) SSTA differences between 2008 and 2007. SSTs are the monthly fields interpolated from the weekly 1° OI analyses of Reynolds et al. (2002). All anomalies are defined as departures from the 1971–2000 climatology (Xue et al. 2003).

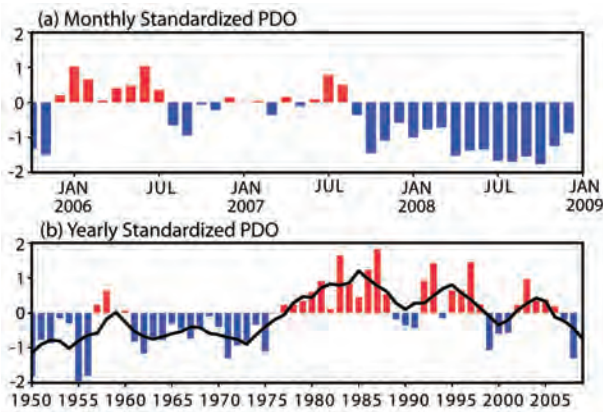


FIG. 3.3. (a) Monthly standardized PDO index (bar) in the past four years and (b) yearly mean of the monthly PDO index (bar) overlapped with the 5-yr running mean of the index (black line) in 1950–2008. The PDO index was downloaded from University of Washington at <http://jisao.washington.edu/pdo>.

persisted through calendar year 2008 (Fig. 3.3a). The longer-term yearly mean PDO index illustrates prominent low-frequency variability with a downward trend from the mid-1980s to the present (Fig. 3.3b). Interestingly, the PDO value in 2008 was the lowest since 1971. Along with the negative PDO phase, upwelling along the west coast of North America was also well above normal during the 2008 upwelling season, which favored high biological productivity during the past year (Frank Schwing 2009, personal communication).

The global mean SST in 2008 was slightly cooler than that in 2007 (Fig. 3.4a), largely due to the cooling in the central tropical Pacific, the Arctic Ocean, and the regions extending from the Gulf of Alaska to the west coast of North America (Fig. 3.2b). The 2008 minus 2007 SSTa differences largely resemble the negative PDO pattern, which is also reflected in the anomaly differences of surface latent plus sensible heat flux (Fig. 3.8b). The tripole SST pattern in the North Atlantic is also reflected in the heat fluxes.

The global mean SST in 2007 and 2008 was much cooler than that during 2002–06 (Fig. 3.4a). The cooling in the past two years was largely due to the cooling in the tropical Pacific (Fig. 3.4b), which is associated with the 2007–08 La Niña and

persistent negative PDO (Fig. 3.3a). The cooling in the tropical Pacific contributed to the cooling in the global tropical oceans in the past two years, although the contributions from the tropical Indian and Atlantic Oceans were less evident (Figs. 3.4c–e). From a historical perspective, the global mean SST was below normal (1971–2000 average) during 1950–76 and has been persistently above normal since 1997. Although the global mean and tropical mean SSTAs all have a prominent upward trend from 1950 to 2008, similar trends are not evident in the North Pacific and North Atlantic (Figs. 3.4f–g).

c. Ocean heat content—G. C. Johnson, J. M. Lyman, J. K. Willis, S. Levitus, T. Boyer, J. Antonov, C. Schmid, and G. J. Goni
Storage and transport of heat in the ocean are central to aspects of climate such as El Niño (e.g., Zebiak 1989), the North Atlantic Oscillation (e.g., Curry

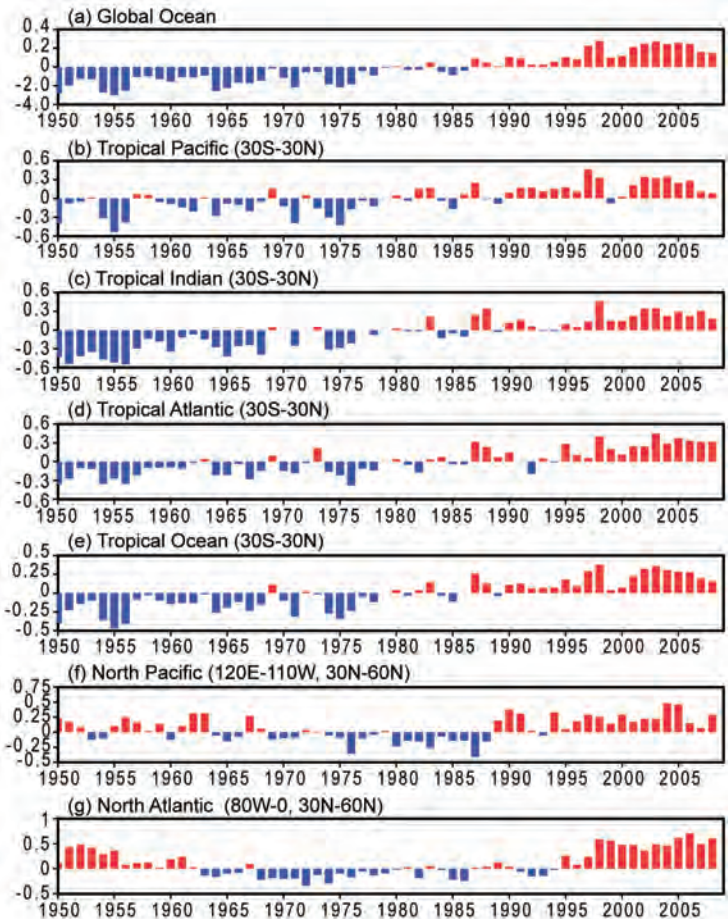


FIG. 3.4. Yearly mean SST anomalies (°C) averaged in (a) the global ocean, (b) tropical Pacific Ocean, (c) tropical Indian Ocean, (d) tropical Atlantic Ocean, (e) all three tropical oceans, (f) North Pacific, and (g) North Atlantic in 1950–2008. SSTs are the ERSST v.3b of Smith et al. (2008). All anomalies are defined as departures from the 1971–2000 climatology (Xue et al. 2003).

and McCartney 2001), hurricanes (e.g., Mainelli et al. 2008; Vecchi et al. 2008), sea level rise (e.g., Domingues et al. 2008), and global warming (e.g., Hansen et al. 2005).

We begin by discussing an estimate of upper (0–750 m) OHCA for the period 1 January–31 December 2008 (Fig. 3.5a) computed from a combination of in situ ocean temperature data and satellite altimetry data, following Willis et al. (2004) but relative to a 1993–2008 baseline, hereafter the combined estimate. We also discuss changes in the combined estimate between 2008 and 2007 (Fig. 3.5b). We contrast these combined estimate changes with changes of mixed layer OHCA (Fig. 3.6) derived from in situ observations (Schmid 2005), hereafter the mixed layer estimate. We also put the estimates of recent upper-OHCA variability into a longer-term context using a time series of global integrals of 0–700-m in situ OHCA from 1955 through 2008 (Fig. 3.7), a

time period much longer than the satellite altimeter record, estimated following Levitus et al. (2009), hereafter the in situ estimate.

In recent years many of the globally distributed in situ subsurface ocean temperature data are from Argo (Roemmich et al. 2004). Data from Argo floats with the potential for as yet uncorrected systematic pressure biases (www.argo.ucsd.edu/Acpres_drift_apex.html) have been removed from the combined estimate presented here. In addition, annual estimates of XBT fall-rate corrections have been applied for deep- and shallow-probe data following Wijffels et al. (2008) for the combined estimate, but with no XBT data used after 2005. A somewhat different set of corrections to MBTs and XBTs for all years is applied for the 0–700-m in situ estimate following Levitus et al. (2009). The mixed layer estimate uses Argo and GTSP (www.nodc.noaa.gov/GTSP/) data subject to Argo real-time quality-control criteria followed by local statistical checks to eliminate remaining outliers. Details of all the fields analyzed here may change after data from floats with potential pressure biases are corrected and made available, after more real-time data are subject to delayed-mode scientific quality control, and as XBT and MBT corrections improve.

The 2008 0–750-m combined estimate of OHCA (Fig. 3.5a) shows eddy and meander variability down to the 100-km mapping scales, as does, to a greater extent, the difference of the 2008 and 2007 combined estimates (Fig. 3.5b). Strong small-scale spatial variability in OHCA fields is associated with the western boundary currents in every gyre, as well as the Antarctic Circumpolar Current. The difference in combined estimates between 2008 and 2007 (Fig. 3.5b) illustrates the large year-to-year variability in ocean heat storage, with changes reaching or exceeding the equivalent of a 95 W m^{-2} magnitude surface flux applied over one year ($\sim 3 \times 10^9 \text{ J m}^{-2}$). Ocean advection likely plays a significant role in many of these changes. Upper OHCA, deep variability, freshwater, and mass signals all contribute to sea level anomalies. Despite this, there are many large-scale visual similarities between upper-OHCA (Fig. 3.5) and sea level (Fig. 3.21) fields in 2008, even relative to their differing baseline periods.

Large-scale patterns are evident in OHCA for 2008 (Fig. 3.5a) and its difference from 2007 (Fig. 3.5b). The central equatorial Pacific is still low in heat content, as it was during 2007 due to a La Niña (Levinson and Lawrimore 2008), and the off-equatorial central and eastern tropical Pacific OHCA values also fell from 2007 to 2008. However, the eastern equatorial Pacific heat content has risen to values slightly above

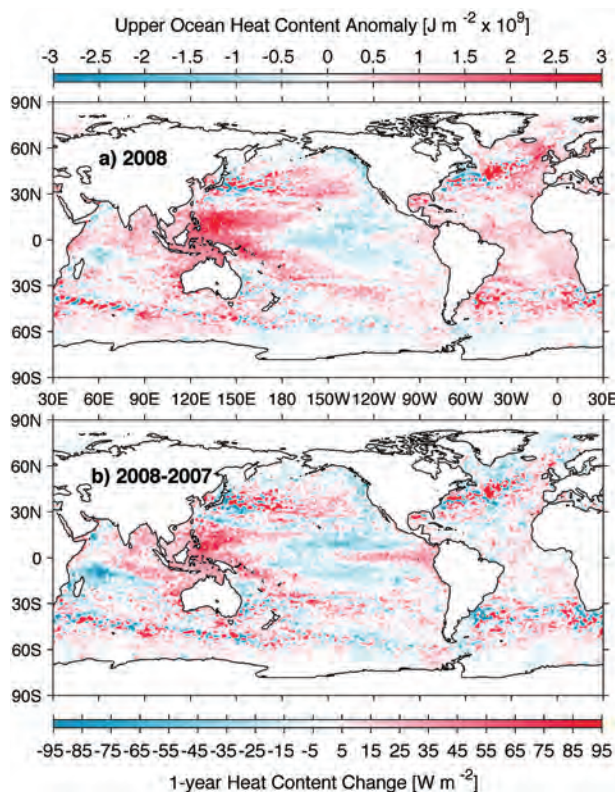


FIG. 3.5. (a) Combined satellite altimeter and in situ ocean temperature data estimate of upper- (0–750 m) ocean heat content anomaly OHCA (10^9 J m^{-2}) for 2008 analyzed following Willis et al. (2004) but relative to a 1993–2008 baseline. (b) The difference of 2008 and 2007 combined estimates of OHCA expressed as a local surface heat flux equivalent (W m^{-2}). For panel comparisons, note that 95 W m^{-2} applied over one year results in a $3 \times 10^9 \text{ J m}^{-2}$ change of OHCA.

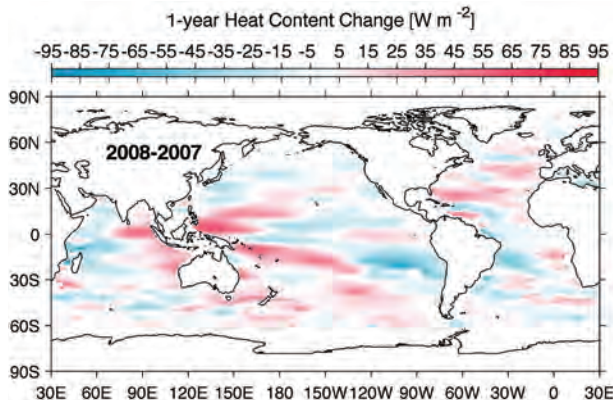


FIG. 3.6. Change of ocean mixed layer heat content estimated following Schmid (2005) expressed as a surface heat flux equivalent (W m^{-2}). The map is based on subtraction of a yearly mean of ocean mixed layer content for calendar year 2008 from that for calendar year 2007.

the mean in that interval, and the western tropical Pacific heat content has risen to levels well above the mean. While the annual averaging period presented here is too long for detailed study of the movement of heat associated with ENSO dynamics, certainly the change on the equator and perhaps those in the off-equatorial regions are related to those processes (e.g., Zebiak 1989).

Like the western tropical Pacific, the northeastern Indian Ocean continued gaining heat between 2007

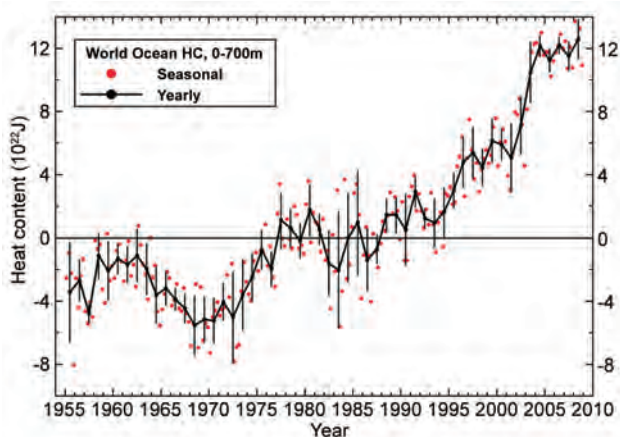


FIG. 3.7. Time series of quarterly (red dots) and annual average (black line) global integrals of in situ estimates of upper OHCA (10^{22} J) for the 0–700-m layer from 1955 to 2008, following Levitus et al. (2009). Error bars for the annual values are 1 std dev of the four quarterly estimates in each year. Additional error sources include sampling errors (Lyman and Johnson 2008) and remaining uncorrected instrument biases (Levitus et al. 2009).

and 2008 (Fig. 3.5b), as both regions did between 2006 and 2007 (Levinson and Lawrimore 2008). As a result, OHCA in the northeastern Indian Ocean in 2008 is above the mean (Fig. 3.5a), contrasting clearly with below-average values found in 2006 (Aguez et al. 2007). Around 10°S in the Indian Ocean heat was lost in the western half and gained in the east from 2007 to 2008 (Fig. 3.5b), largely the reverse of the tendency in this region from 2006 to 2007 (Levinson and Lawrimore 2008), leaving the area around the Seychelles slightly below the mean for OHCA in 2008 (Fig. 3.5a).

The North Pacific shows high OHCA in its center in 2008, and low OHCA off the west coast of North America (Fig. 3.5a). This pattern is consonant with a strongly negative Pacific decadal oscillation (Mantua et al. 1997) during 2008, and hence mirrored in sea surface temperature anomalies for 2008 (Fig. 3.2). The band of high OHCA near 35°S in the South Pacific (Fig. 3.5a) appears to have steadily migrated south from lower subtropical latitudes in 2007 (Fig. 3.5b), and even lower tropical latitudes in 2006 (Aguez et al. 2007).

In the subpolar North Atlantic, the Labrador and Irminger Seas cooled between 2007 and 2008 (Fig. 3.5b), returning OHCA values in these areas to near the 1993–2008 mean (Fig. 3.5a), consonant with a return of deep wintertime convection there in early 2008 (Våge et al. 2009). A strong warming centered near 45°N , 45°W (Fig. 3.5b) suggests a local northwestward shift in the North Atlantic Current in 2008 relative to the previous year. The continued high OHCA values in the eastern subpolar North Atlantic (Fig. 3.5a) suggest that subtropical influences are still strong there, consistent with anomalously salty surface conditions in that region in 2008 (Fig. 3.13). The subtropical and tropical Atlantic in both hemispheres remains slightly warmer than the mean, with little change from 2007 to 2008.

Near the Antarctic Circumpolar Current, OHCA is highly variable (Fig. 3.5a) and appears anomalously cool in the Pacific, warm in the Indian, and mixed in the Atlantic in 2008, a less coherent pattern than in the previous few years (Arguez et al. 2007; Levinson and Lawrimore 2008). This lack of coherence may be related to a shift in the Antarctic Oscillation Index to positive in 2008, after several years of negative values.

A map of year-to-year changes in mixed layer OHCA (Fig. 3.6) shows many similarities to the map of 2008–07 0–750-m combined OHCA (Fig. 3.5b). However, the figures are not directly comparable. The mixed layer map (Fig. 3.6) is much smoother than the analogous combined OHCA map (Fig. 3.5b) because

the former map uses much longer decorrelation length scales (20° lon and 4° lat) than the latter. The difference in scales arises because the combined maps of 0–750-m OHCA use altimeter data to increase resolution and fill in where in situ data are sparse.

These methodological differences notwithstanding, the magnitudes of year-to-year changes in the mixed layer (Fig. 3.6) are generally smaller than those from the combined estimates for 0–750 m (Fig. 3.5b). This reduction in magnitude is expected because year-to-year OHCA changes can extend below the mixed layer. In addition, there are a few regions with qualitative differences in the two quantities, such as on either coast of South America around 20°S, where the mixed layer heat content anomaly has fallen over the course of a year (Fig. 3.6), but there is no such change evident in the combined map of upper OHCA (Fig. 3.5b). Changes in mixed layer depth can have large impacts on the heat content in the mixed layer even if there is no change in the mixed layer temperature, and that fact could be the reason for such striking differences.

Over a multidecadal period, upper-ocean estimates (0–700 m) of in situ ocean heat content following Levitus et al. (2009) reveal a large increase in global integrals of that quantity (Fig. 3.7). Global integrals of the in situ estimates for the last several years have reached consistently higher values than for all prior times in the record. The recent several-year plateau has smaller variability than the rest of the record, probably because of the effects of the excellent data coverage (Lyman and Johnson 2008) as provided by Argo floats (Roemmich et al. 2004). However, there are also long stretches in the record prior to 2000 that also exhibit little upward trend in OHCA.

Finally, around Antarctica and in the northern North Atlantic, near-surface water becomes dense enough to sink to the abyssal ocean, spreading around the globe (e.g., Lumpkin and Speer 2007). The ocean below the 2-km target depth for Argo profiles is not frequently sampled, making quantitative annual global estimates of abyssal ocean heat content changes impossible. However, there is observational evidence that the deep oceans, including the North Atlantic, have gained heat at least to 3,000 m over the past few decades (Levitus et al. 2005). Furthermore, analyses of recent repeated hydrographic observations in the deep South Atlantic (Johnson and Doney 2006), Pacific (Johnson et al. 2007), and South Indian Oceans (Johnson et al. 2008a) suggest that Antarctic Bottom Water has warmed over the last decade and that this warming could make a contribution to the global heat budget on the order of 10%–20%.

d. Global ocean heat fluxes—L. Yu and R. A. Weller

Much of the solar energy absorbed at the top ocean layer is released back to the atmosphere by two heat exchange processes at the air–sea interface: evaporation that releases latent heat and conduction and convection that releases sensible heat. These air–sea heat exchanges cool the ocean but warm the air, supplying the heat energy needed to drive the atmospheric circulation and global weather patterns. Clearly, air–sea heat fluxes (i.e., the amount of air–sea heat exchange) are a key measure of the role that the ocean plays in global climate, and their changes on short-term and long-term time scales may have important climate implications.

The global distribution of latent and sensible heat fluxes in 2008 (Fig. 3.8a) shows that on an annual basis the largest ocean heat losses occur over the regions associated with major WBCs and their extensions (e.g., the Kuroshio off Japan, the Gulf Stream off the United States, and the Agulhas Current off the African coast). The magnitude of the annual mean LHF + SHF in these regions exceeds 250 W m^{-2} , produced largely during the fall-to-winter seasons by strong winds and cold and dry air masses coming from the land (Bigorre and Weller 2008). The second-largest heat loss ($\sim 180 \text{ W m}^{-2}$) is located over the broad subtropical southern Indian Ocean, where the large air–sea heat exchange is sustained primarily by the strong southeast trade winds in the monsoon months June–September.

The estimates of LHF + SHF were produced by the OAFlux project (Yu et al. 2008) at WHOI. The computation of the OAFlux products uses the state-of-the-art bulk flux algorithm version 3.0 by Fairall et al. (2003), with the surface meteorological variables determined from an optimal blending of satellite retrievals and atmospheric reanalysis/forecast models of NCEP and ECMWF. The accuracy of the OAFlux LHF and SHF estimates was evaluated using 105 buoys available over the global oceans (Yu et al. 2008, manuscript submitted to *J. Climate*). The averaged root-mean-square differences between OAFlux and buoy calculated over the buoy locations are 9.6 W m^{-2} for LHF and 2.6 W m^{-2} for SHF.

The plot of the LHF + SHF differences between 2008 and 2007 (Fig. 3.8b) shows that LHF + SHF had significant changes in the tropical Pacific and Indian Oceans. Positive anomalies are observed in the equatorial eastern Pacific and central tropical Indian Oceans, while negative anomalies are found in the central tropical Pacific. These changes appear to result from the direct response of LHF to SST. The equatorial Pacific in the second half of 2008 was in

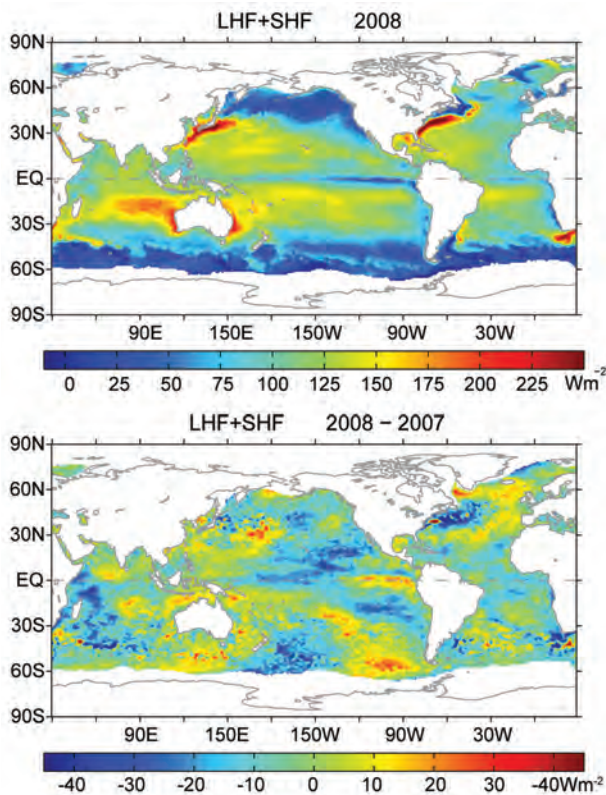


FIG. 3.8. (top) Annual mean latent plus sensible heat fluxes in 2008. The sign is defined as upward (downward) positive (negative). (bottom) Differences between the 2008 and 2007 annual mean latent plus sensible heat fluxes.

ENSO-neutral conditions after a La Niña faded in the spring. The eastern equatorial Pacific warmed following the cool La Niña conditions and the central equatorial Pacific cooled (Fig. 3.2b). Because a warmer (cooler) sea surface increases (reduces) the rate of heat transfer by evaporation, more (less) latent heat was lost in the eastern (central) equatorial Pacific as the basin evolved from a cold ENSO phase to an ENSO-neutral phase. On the other hand, unlike the Pacific counterpart, SST was not the leading cause of the larger LHF in the central tropical Indian Ocean. Persistent dry westerly wind anomalies associated with enhanced convection over the Maritime Continent contributed to a faster rate of evaporation over the warm tropical Indian Ocean waters.

While the tropical Pacific returned to an ENSO-neutral state, the basin-scale pattern of the Pacific was locked in a cool phase of the PDO (Mantua et al. 1997) that started in 2007 (<http://jisao.washington.edu/pdo/PDO.latest>). The PDO in 2008 was the most negative since 1971. Compared to 2007, SST had trended downward in a much broader area off the coast of North America from Alaska to the equator, forming a

cool horseshoe-shape region around a core of warmer SST anomalies to the west (Fig. 3.2b). Interestingly, the LHF + SHF 2008 minus 2007 difference pattern in the Pacific bears a broad resemblance to the classic pattern of the cool PDO phase, with enhanced (reduced) latent and sensible heat loss over positive (negative) SST anomalies. The positive correlation between SST and LHF + SHF is indicative of the atmospheric response to SST, underlying the dominant role of the ocean in the large-scale atmospheric circulation in the Pacific.

For the North Atlantic Ocean, the LHF + SHF difference anomalies between 2008 and 2007 show a tripole structure, with negative anomalies off the east coast of North America (between 30° and 60°N) and positive anomalies to its north and south. The pattern is similar to that of the SST difference anomalies (Fig. 3.2b), but the sign is opposite. This negative correlation between SST and LHF + SHF implies that the variability of the Atlantic SST in 2008 was driven primarily by the atmospheric forcing: SST increases (decreases) as a result of reduced (enhanced) latent and sensible heat loss at the sea surface. That heat fluxes are important forcing for the North Atlantic Ocean variability in 2008 was best demonstrated by a recent study by Våge et al. (2009), who reported a remarkable deep convective overturning event in the Labrador and Irminger Seas in the winter of 2007/08 (defined as December 2007 to February 2008), triggered by rapid, intensive sea surface cooling under unusually cold westerly winds. Deep convection in the northern North Atlantic is regarded as a pump that drives the Atlantic meridional overturning circulation, and it has been suggested that its onset depends on strong westerly winds across this ocean basin that occur during the positive phase of the NAO (Hurrell et al. 1995). Våge et al. (2009) showed that winter 2007/08 was unusual. Though the NAO index was lower than in the previous winters, the westerly winds were unusually strong and cold, resulting in very large latent and sensible heat loss at the sea surface and subsequently a mixing of the water column to depths that had not been reached since the mid-1990s. This enhanced flux of ocean heat in the 2007/08 winter, which was more than 100 W m^{-2} above the winter climatology (Våge et al. 2009), left a clear mark even on the difference plot based on the 2007 and 2008 annual means (Fig. 3.8b): a band of positive LHF + SHF anomalies extends eastward from the ice edge in the Labrador Sea into the Irminger Sea.

The changing relationships between air-sea fluxes and SST from the Pacific to the Atlantic Oceans provide a clear example that the global climate system is

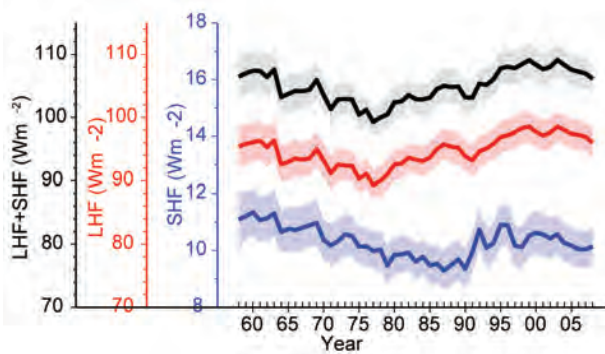


FIG. 3.9. Year-to-year variations of global-averaged annual mean latent plus sensible heat flux (blue line), latent heat flux (red line), and sensible heat flux (black line). The shaded areas indicate the upper and lower limits at the 90% confidence level.

ruled by intricate feedbacks between the ocean and the atmosphere. The oceans modulate large-scale climate variability and change, while short-term weather events could impose significant impact on ocean variability and thus impart an indelible signature on the long-term climate of the ocean circulation. It is worth noting that changes in air–sea heat fluxes also affect the hydrological cycle and hence ocean salinity, as the evaporation releases not only latent heat but also water vapor to the atmosphere. The structure of LHF + SHF anomalies, in particular the tripole shape in the North Atlantic Ocean, was in broad agreement with that of surface salinity anomalies (Fig. 3.13b). The freshening of the sea surface (i.e., negative surface salinity anomalies) over the Gulf Stream was in tune with the local weakened evaporation (i.e., negative LHF + SHF anomalies), while the increased surface salinity to the north and south coincided with enhanced evaporation forcing (positive LHF + SHF anomalies).

The basin-averaged LHF + SHF in 2008 was slightly down from 2007, continuing the broad downward trend that started in 1999 (Fig. 3.9). There seems to be a tendency toward reversing the upward trend that had dominated the decades of 1980s and 1990s.

e. *Tropical cyclone heat potential*—G. J. Goni and J. A. Knaff

Tropical cyclones occur in seven regions in all ocean basins: tropical Atlantic, northeast Pacific, northwest Pacific, southwest Indian, north Indian, southeast Indian, and South Pacific. While SST plays a role in the genesis of TCs, the ocean heat content contained between the sea surface and the depth of the 26°C isotherm, also referred to as TCHP, has been shown to play a more important role in TC

intensity changes (Shay et al. 2000), provided that atmospheric conditions are also favorable. The TCHP shows high spatial and temporal variability associated with oceanic mesoscale features. Sea surface height observations derived from satellite altimetry can be used to compute the TCHP (Goni et al. 1996; Shay et al. 2000). In general, the real-time forecast of TC intensity is highly dependent on track forecasts, and many of the errors introduced in the track forecast are translated into the intensity forecast. Clearly, areas with high values of TCHP may be important only when TCs travel over them.

To examine the interannual variability of TCHP with respect to tropical cyclones, TCHP anomalies are computed during the months of TC activity in each hemisphere: June through November in the Northern Hemisphere and November through April in the Southern Hemisphere. Anomalies are defined as departures from the mean TCHP calculated during the same months for the period 1993 to 2008. These anomalies show large variability within and among the tropical cyclone basins (Fig. 3.10).

The west Pacific basin exhibits the anomalies from the signature of the negative phase of the 2007 ENSO event (La Niña). The South Pacific basin showed mostly positive anomalies. The north Indian Basin exhibited positive values in the Bay of Bengal and in the eastern Arabian Sea and negative values in the

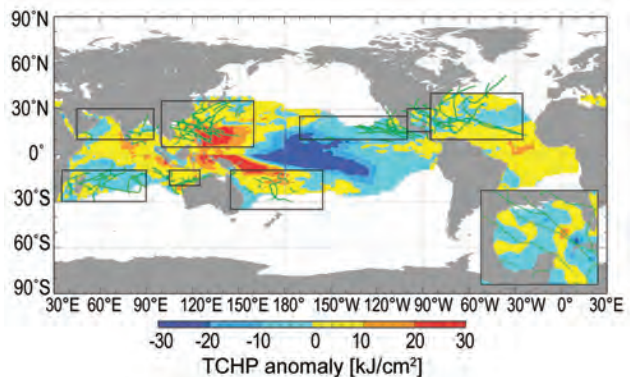


FIG. 3.10. Global anomalies of TCHP corresponding to 2008 computed as described in the text. The boxes indicate the seven regions where TCs occur: (left to right) southwest Indian, north Indian, west Pacific, southeast Indian, South Pacific, east Pacific, and North Atlantic (shown as Gulf of Mexico and tropical Atlantic separately). The black lines indicate the trajectories of all tropical cyclones Category 1 and above during Nov 2007 through Dec 2008 in the Southern Hemisphere and Jan through Dec 2008 in the Northern Hemisphere. The Gulf of Mexico conditions during Jun through Nov 2008 are shown in detail in the insert shown in the lower right corner.

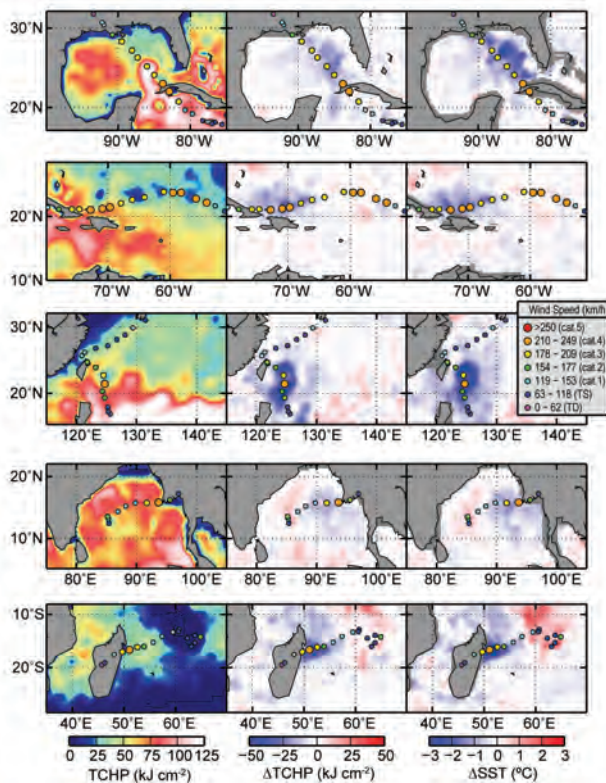


FIG. 3.11. (left) Tropical cyclone heat potential and surface cooling given by the difference between post- and prestorm values of (center) tropical cyclone heat potential and (right) sea surface temperature, for (from top to bottom) Hurricane Gustav, Hurricane Ike, Typhoon Sinlaku, Tropical Cyclone Nargis, and Tropical Cyclone Ivan.

western Arabian Sea. The Gulf of Mexico (insert) showed an alternation of regions with positive and negative values. The tropical Atlantic exhibited positive values to the north of 30°N and south of 15°N . The most evident changes that happened between 2008 and 2007 are the increase of values in the southern region of the western Pacific basin.

During 2008 several TCs were identified to have gained strength when traveling into regions of very high or higher values of TCHP. Some examples of these intensification events are shown in Fig. 3.11. The results presented here correspond to five intense (Categories 4 and 5) TCs, where the location of their intensification coincided with an increase of the values of TCHP along their tracks. Additionally, the cooling associated with the wake of the TCs, which can reach values of 30 kJ cm^{-2} in tropical cyclone heat potential and 3°C in sea surface temperature, is important because it influences the upper-ocean thermal structure on regional scales within weeks to months after the passage of the cyclones. These TCs were Gustav in the

Gulf of Mexico, Ike in the Caribbean Sea, Sinlaku in the western Pacific, Nargis in the northern Indian, and Ivan in the southwest Indian region. A brief description of each of these storms is now presented.

In the Atlantic basin, Hurricanes Gustav and Ike are good examples of major hurricanes that interacted with TCHP features. Hurricane Gustav (25 August–2 September) reached its maximum estimated intensity of 125 kt prior to making landfall in Cuba on 30 August and at a time when its track was traversing some of the highest values of TCHP west of Jamaica. The storm's impact was felt throughout the northern Caribbean in Hispanola, Jamaica, the Cayman Islands, and Cuba. On the other hand, Hurricane Ike (1–14 September) experienced three separate peak intensities. The first and maximum peak intensity, 125 kt, was obtained in the central Atlantic, northwest of the Leeward Islands. In the next day or so, the storm weakened and moved southwest. The second peak shown in Fig. 3.11 occurred in a region of elevated TCHP. The third peak intensity occurred in the Gulf of Mexico before making landfall in Texas (not shown in Fig. 3.11). This storm resulted in major impacts throughout the northern Caribbean, making landfall twice in Cuba (110, 115 kt) and once in Texas (95 kt).

Typhoon Sinlaku (8–22 September), in the western North Pacific, obtained its maximum intensity (125 kt) following an encounter with a warm ocean eddy. Following its peak intensity, the storm weakened slightly as it turned toward Taiwan and moved over lower values of TCHP. Following this weakening, Sinlaku showed a slight intensification as it tracked to the northwest and moved over larger TCHP values. The storm eventually brushed the northeast coast of Taiwan on 13 September with an estimated intensity between 90 and 95 kt.

In the north Indian Ocean, Tropical Cyclone Nargis (27 April–3 May) made landfall in Myanmar on 2 May with an estimated intensity of 115 kt. The storm resulted in a devastating surge that killed an estimated 146,000 people. The storm intensified over the high TCHP waters of the Bay of Bengal. One aspect of the storm's forecast is that for the 48 h prior to landfall the storm was forecasted to have a more northward track than was observed, which not only allowed the storm to track over higher TCHP values but to make landfall in the low-lying Irrawaddy River delta. This storm occurred in early May and likely contributed to the negative anomalies in Fig. 3.10 in the northern part of the Bay of Bengal.

Tropical Cyclone Ivan (7–22 February) is a good example of a very strong and rather large Southern Hemisphere tropical cyclone, which reached its

maximum intensity of 115 kt just as it made landfall in Madagascar. Ivan also tracked across the warmest TCHP during the day or so prior to landfall on 17 February when intensification was occurring. Initial reports indicated that 26 deaths occurred and more than 300,000 persons were affected, particularly by the heavy general rainfall and subsequent floods in the north and east of the island of Madagascar.

Hurricane Gustav (2008) is now contrasted with Hurricane Katrina (2005) (Fig. 3.12). Both hurricanes made landfall in a region in the Gulf of Mexico. There are some similarities as they both traveled directly over the Loop Current. Katrina was energized by its passage over the Loop Current and continued to intensify as it moved from the Loop Current region into a region occupied by a warm ring shed by the Loop Current. The storm also became larger as it went through an eyewall replacement cycle (Maclay et al. 2009). Gustav, in contrast, tried to reorganize over the Loop Current region following a landfall in western Cuba, but instead of moving over a warm eddy as Katrina did, Gustav moved into a region of relatively low TCHP and did not reintensify despite being in favorable environmental conditions (200–850-hPa vertical wind shear <15 kt and SST >29°C). As a likely consequence, Gustav did not become nearly as large or as intense as Katrina. And while both storms weakened as they approached the Louisiana coast, Katrina with its larger and more intense wind field and landfall in a more populated area produced more property damage. The difference in the intensity of these two hurricanes translates into a difference in sea surface cooling. Maximum cooling by Katrina was approximately 30 kJ cm⁻² in tropical cyclone heat potential and 4°C in sea surface temperature, almost double that observed for Hurricane Gustav.

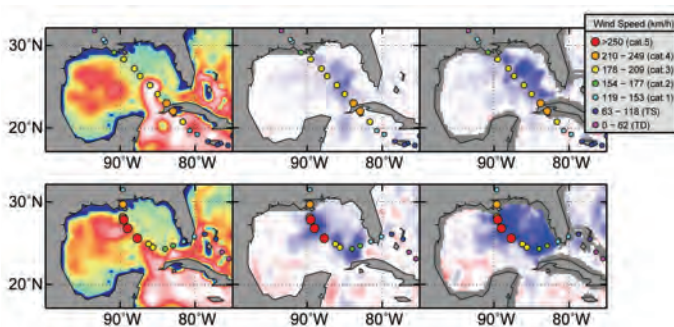


FIG. 3.12. (left) Tropical cyclone heat potential and surface cooling given by the difference between post- and prestorm values of (center) tropical cyclone heat potential and (right) sea surface temperature, for Hurricanes (bottom) Katrina in 2005 and (top) Gustav in 2008. The scales are the same as in Fig. 3.11.

f. Sea surface salinity—G. C. Johnson and J. M. Lyman

Ocean storage and transport of freshwater are intrinsic to aspects of global climate including the water cycle (e.g., Wijffels et al. 1992), El Niño (e.g., Maes et al. 2006), and anthropogenic climate change (e.g., Held and Soden 2006). In the past, in situ ocean salinity data have been too sparse and their reporting too delayed for an annual global perspective of ocean freshwater and its complement, salinity. However, over the past few years, the now mature Argo array of profiling floats, which measures temperature and salinity year-round in the upper 2 km of the ice-free global ocean (Roemmich et al. 2004), has remedied this situation. In addition, remote sensing of SSS by satellite is planned for 2010 (<http://aquarius.gsfc.nasa.gov/>).

The near-global Argo data are analyzed here to determine an annual average SSS anomaly for 2008 relative to a climatology and to describe how annual SSS anomalies have changed in 2008 relative to 2007. In this work the shallowest near-surface (<25 m) salinity data flagged as good from each available Argo profile for 2007 and 2008 were subjected to a statistical check to discard outliers. After this statistical check, the remaining data were then cast as differences from a climatological mean surface salinity field from the WOA based on historical data reported through 2001 (WOA 2001; Boyer et al. 2001). The resulting anomalies were then mapped (Bretherton et al. 1976) assuming a Gaussian covariance function with 6° latitude and longitude decorrelation length scales and a noise-to-signal variance ratio of 2.2. While some delayed-mode scientific controlled (final) Argo data are available for the 2007–08 time period, many real-time (preliminary) Argo data were used in both years. The real-time estimates of SSS made here could change after all the data have been subjected to careful scientific quality control.

Climatological SSS patterns are correlated with surface freshwater flux: the sum of evaporation, precipitation, and river runoff (e.g., Báranger et al. 1999) where advection processes are not dominant. In each ocean basin, subtropical salinity maxima centered between roughly 20° and 25° in latitude are signatures of the predominance of evaporation over precipitation. Conversely, in most regions where climatological surface salinities are relatively fresh, such as the high latitudes and the ITCZs, precipitation generally dominates over evaporation.

The 2008 anomalies from WOA 2001 (Fig. 3.13a) reveal some large-scale patterns

that also hold in 2005 through 2007 (not shown). The regions around the subtropical salinity maxima are mostly salty with respect to WOA 2001. Most of the high-latitude climatologically fresh regions appear fresher than WOA 2001, including most of the ACC near 50°S and the subpolar gyre of the North Pacific. These patterns may be consistent with an increase in the hydrological cycle (i.e., more evaporation in drier locations and more precipitation in rainy areas), as seen in simulations of global warming. These simulations suggest this signal might be discernible over the last two decades of the twentieth century (Held and Soden 2006), consistent with the multiyear nature of these anomalies. In addition, a study of global subsurface salinity anomalies comparing 2000 Argo data to those from the 1990 World Ocean Circulation Experiment and prior historical data suggests that these patterns are persistent and decadal (K. P. Helm et al. 2009, manuscript submitted to *Nature Geosci.*).

Nonetheless, there may be alternate explanations. It is possible that the climatology, being based on relatively sparse data distributions in many parts of the oceans, may tend to underestimate regional extrema that the well-sampled Argo array can better resolve, or that the climatology contains regional biases on seasonal or longer time scales that are not present in the Argo data. Also, some of these patterns might be explained by interannual variability in large-scale oceanic currents or atmospheric features such as the ITCZs.

For example, in contrast to the other high-latitude areas, the subpolar North Atlantic and Nordic Seas in 2008 are anomalously salty with respect to WOA 2001 (Fig. 3.13a), as they have been since at least 2005 (not shown). This salty subpolar anomaly is inconsistent with a simple increase in the strength of the hydrological cycle. However, the pattern may have less to do with local evaporation and precipitation fields than with northward spread of saltier waters from the south. The salty anomaly in this region is consistent with a stronger influence of subtropical gyre waters in the northeastern North Atlantic in recent years and a reduced extent of the subpolar gyre (Hátún et al. 2005).

Salinity in the tropics exhibits strong interannual variability due to influences of phenomena such as the ENSO cycle (e. g., Ando and McPhaden 1997). For instance, the ITCZ in the central and eastern tropical Pacific is anomalously salty in 2008 (Fig. 3.13a), with some of that anomaly due to changes since 2007 (Fig. 3.13b), probably caused by an ongoing La Niña in 2008 reducing atmospheric convection and thus changing patterns of evaporation (Fig. 3.8) and precip-

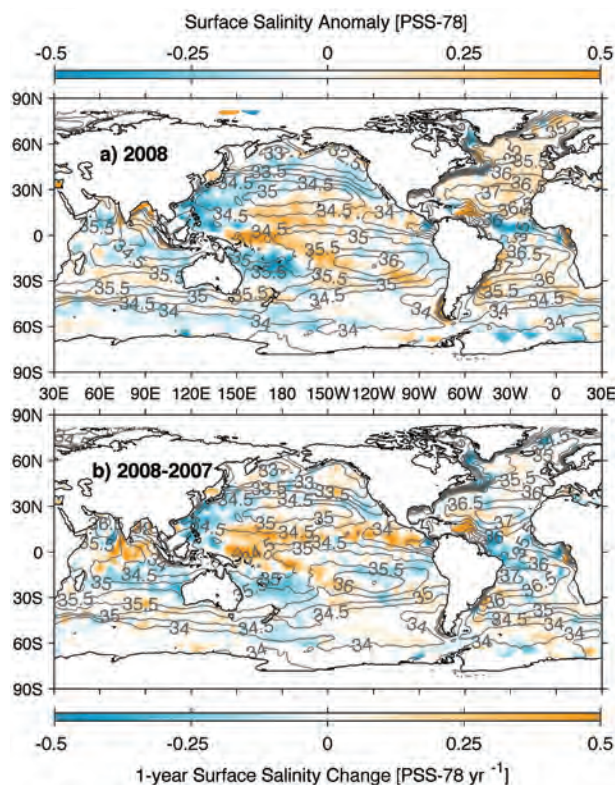


FIG. 3.13. (a) Map of the 2008 annual surface salinity anomaly estimated from Argo data (colors in PSS-78) with respect to a climatological salinity field from WOA 2001 (gray contours at 0.5 PSS-78 intervals). (b) The difference of 2008 and 2007 surface salinity maps estimated from Argo data [colors in PSS-78 yr⁻¹ to allow direct comparison with (a)]. White areas are either neutral with respect to salinity anomaly or too data poor to map. While salinity is often reported in PSU, it is actually a dimensionless quantity reported on the PSS-78.

itation in the region. In contrast, freshening in the far western tropical Pacific is evident, as is freshening in the Atlantic ITCZ. In addition, a strong fresh anomaly south of India in the tropics in 2007 (not shown) is absent in 2008 (Fig. 3.13a), again due to changes taking place over a 1-yr interval (Fig. 3.13b).

g. Surface current observations—R. Lumpkin, G. Goni, and K. Dohan

Near-surface currents are measured in situ by drogued¹ satellite-tracked drifting buoys and by current meters on moored ATLAS buoys. (Drifter

¹ A drogued buoy is attached to a large cylindrical canvas sea anchor. The drogue (sea anchor) dominates the surface area of the drifter and ensures that it follows currents at the drogue depth of 15 m rather than being blown by the wind.

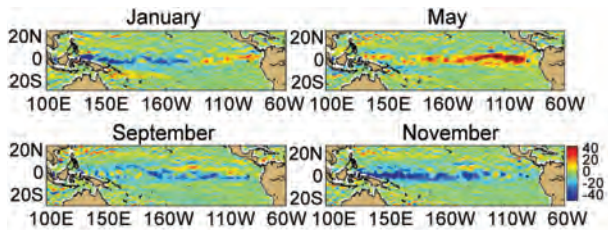


FIG. 3.14. OSCAR monthly averaged zonal current anomalies (cm s^{-1}), positive eastward, with respect to seasonal climatology for Jan, May, Sep, and Nov 2008.

data are distributed by NOAA/AOML at www.aoml.noaa.gov/phod/dac/gdp.html. Moored data are distributed by NOAA/PMEL at www.pmel.noaa.gov/tao. OSCAR gridded currents are available at www.oscar.noaa.gov/. AVISO gridded altimetry is produced by SSALTO/DUACS and distributed with support from CNES, at www.aviso.oceanobs.com/) During 2008, the drifter array ranged in size from a minimum of 918 drogued buoys to a maximum of 1,065, with a median size of 966 drogued buoys (undrogued drifters continue to measure SST but are subject to significant wind slippage; Niiler et al. 1987). The moored array included 35 buoys with current meters, all but two between 10°S and 21°N . Tropical moorings are maintained by the Pacific Ocean TAO, Atlantic Ocean PIRATA, and Indian Ocean RAMA projects. The two nontropical moored current meter sites of the Global Ocean Observing System are the Kuroshio Extension Observatory (32°N , 145°E) and Ocean Station Papa (50°N , 145°W).

Satellite-based estimates of ocean currents are produced by NOAA's OSCAR project, which uses satellite altimetry, winds, and SST to create 1° resolution surface current maps for the 0–30-m layer of the ocean (Bonjean and Lagerloef 2002). Anomalies are calculated with respect to the time period 1992–2002.

1) SURFACE CURRENT ANOMALIES IN 2008

The instantaneous distribution of current anomalies from the 1992–2002 mean mainly reflects the distribution of eddy kinetic energy associated with mesoscale eddies (cf., Stammer 1998; Lumpkin and Pazos 2007). To be significant, we require that anomalies must exceed the mean standard deviation (square root of eddy kinetic energy) with a distribution extending over several Eulerian length scales (Stammer 1998). By this definition, the only significant short-term (seasonal

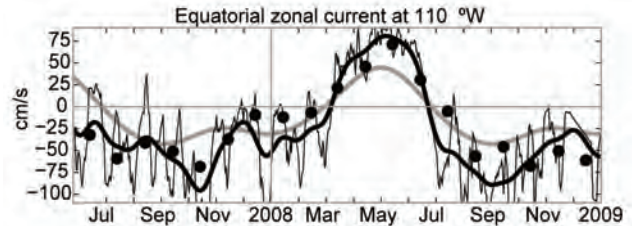


FIG. 3.15. Daily (thin black) and 15-day low-passed (thick black) zonal currents (positive eastward) measured at the equatorial TAO mooring at 110°W , at a depth of 10 m. Also shown are the mean seasonal cycle (gray) and OSCAR monthly mean zonal currents (black dots) at this location.

to annual) anomalies in 2008 occurred in the tropical Pacific Ocean. Longer-term variations can be resolved elsewhere and are discussed in the next section.

In the equatorial Pacific, the year began with large westward current anomalies in the western basin, associated with strong La Niña conditions, extending to 140°W (Fig. 3.14). In the eastern basin, weak eastward anomalies were seen from 120°W to the South American coast. These eastward anomalies grew in intensity and spatial coverage despite enhanced easterly surface winds (Fig. 4.4) At 110°W , this eastward anomaly pattern peaked in early May (Fig. 3.15), when the seasonal cycle typically reaches its maximum eastward speed. The eastward anomalies were $20\text{--}40 \text{ cm s}^{-1}$ above typical May values and extended from South America to 160°E (Fig. 3.14). These anomalies deepened the thermocline in the eastern equatorial Pacific (Fig. 4.3),

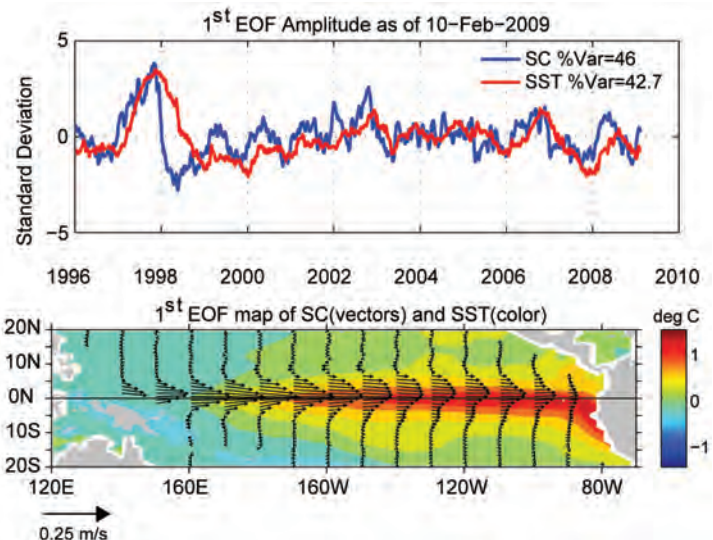


FIG. 3.16. Principal EOF of surface current (“SC”) and SST anomaly variations in the tropical Pacific. (top) Amplitude time series of the EOFs normalized by their respective std devs. (bottom) Spatial structures of the EOFs.

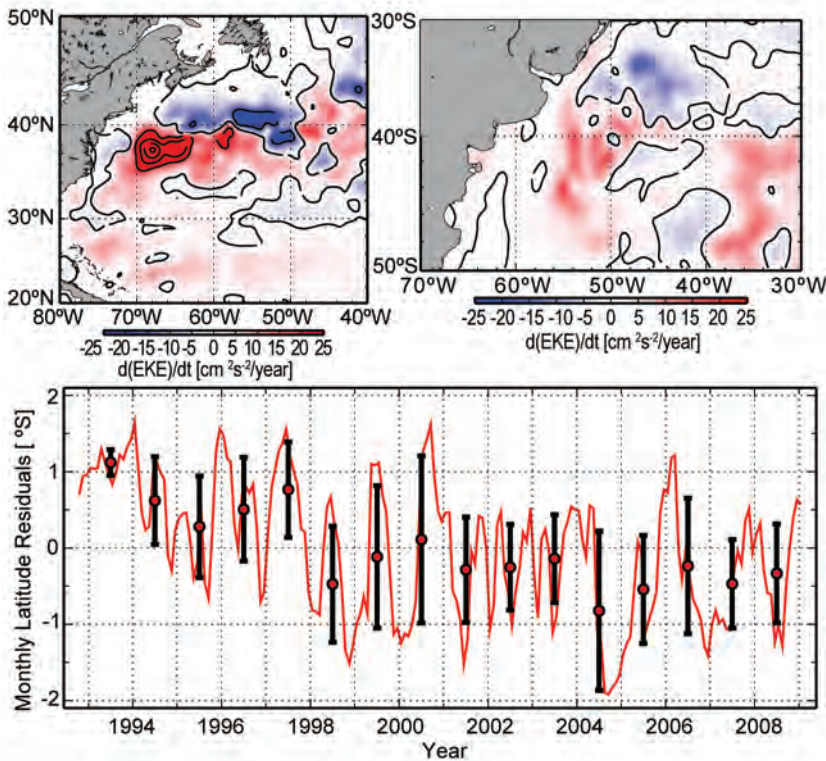


FIG. 3.17. Trends in geostrophic EKE for 1993–2008 in (top left) the Gulf Stream region and (top right) the Brazil–Malvinas Confluence, calculated from satellite altimetry. (bottom) Location of the Brazil Current separation with respect to its mean position over the period 1993–2008. Circles with bars indicate annual means and 2 std devs of the values in each calendar year.

increasing upper-ocean heat content and resulting in warm SST anomalies (Fig. 4.2). Warm SSTs were concentrated west of 120°W on the equator in May, when the Niño-3.4 index (which had been negative from January–April) became neutral (Fig. 4.1).

This El Niño–like surface current pattern, associated with the transition from La Niña to ENSO-neutral conditions, weakened in early boreal summer and had disappeared by early fall when warm SST anomalies in the eastern equatorial Pacific peaked and the monthly averaged Niño-3 and Niño-3.4 indices reached their maximum 2008 value (Fig. 4.1).

Through midboreal summer, westward current anomalies developed in the eastern part of the Pacific basin, reaching a peak of 40 cm s⁻¹ (with respect to seasonal climatology) in September at 110°W (Fig. 3.15; anomaly is difference between the black and gray curves). This pattern spread westward in late 2008, reaching the western Pacific with maximum anomalies of 65–75 cm s⁻¹ in November (Fig. 3.14). The resulting shallower thermoclines in the eastern Pacific were associated with cool SST anomalies and decreases in the Niño-3 and Niño-3.4 indices over

the period October–December (Fig. 4.1).

Surface current anomalies in the equatorial Pacific typically lead SST anomalies by several months, with a magnitude that scales with the SST anomaly magnitude. Recovery to normal current conditions is also typically seen before SST returns to normal. Thus, current anomalies in this region are a valuable predictor for the evolution of SST anomalies and their related climate impacts. This leading nature can be seen clearly in the first principal EOF of surface current anomaly and separately of the SST anomaly in the tropical Pacific basin (Fig. 3.16), extending back to 1996.

2) LONG-TERM CHANGES IN SURFACE CURRENTS

Geostrophic EKE can be derived from gridded AVISO altimetry fields and reveals long-term trends in the Atlantic Ocean over the period 1993–2008 that may indicate a change of intensity and

location of major surface currents. Along the axis of the Gulf Stream (Fig. 3.17) an increase in EKE to the south and a decrease to the north may indicate a long-term shift to the south in the current. In the southwestern Atlantic, a similar situation occurs, where the linear trend of EKE exhibits negative (positive) values to the north (south) of 38°S in the Brazil–Malvinas Confluence region. As with the Gulf Stream, this linear trend may indicate a shift in the surface current field to the south. Altimetry observations (bottom, Fig. 3.17) also show that the separation of the Brazil Current from the continental shelf break (Goni and Wainer 2001) has shifted south over the period 1993–2008. However, since 2004 (when the Brazil Current reached its southernmost separation point) it has tended to shift to the north.

h. The meridional overturning circulation—M. O. Baringer, C. S. Meinen, G. C. Johnson, T. O. Kanzow, S. A. Cunningham, W. E. Johns, L. M. Beal, J. J.-M. Hirschi, D. Rayner, H. R. Longworth, H. L. Bryden, and J. Marotzke

The meridional redistribution of mass and heat associated with the large-scale vertical circulation with-

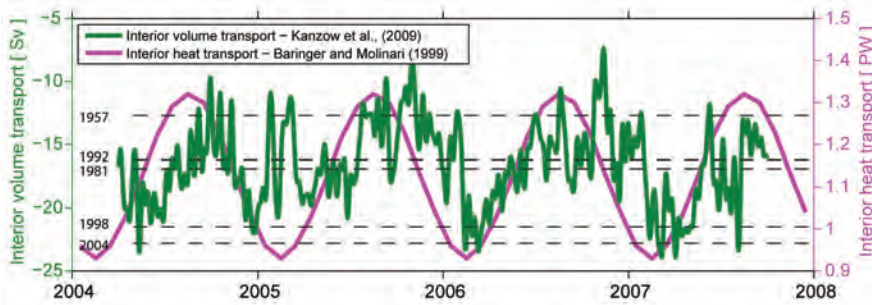


FIG. 3.18. Daily estimates of the strength of the upper 1,000-m transport (green solid) as measured by the United Kingdom’s NERC Rapid Climate Change Program, the National Science Foundation’s Meridional Overturning and Heat transport Array, and the long-term NOAA-funded Western Boundary Time Series Program. The interior volume transport estimate (accurate to 1 Sv; Cunningham et al. 2007) is based on the upper-ocean transport from Mar 2004 to Oct 2007 (adapted from Fig. 7 from Kanzow et al. 2009), with a 10-day low-pass filter applied to the daily transport values. Dashed black horizontal lines are the Bryden et al. (2005) upper-ocean transport values from the 1957, 1981, 1992, 1998, and 2004 transatlantic hydrographic sections. The total heat transport (estimated error 0.2 PW for monthly averages) is adapted from Baringer and Molinari (1999), including the mean heat transport components from Molinari et al. (1990).

in the oceans is typically called the MOC. The most common definition of the strength of the MOC at any particular latitude is the maximum of the vertically integrated basin-wide streamfunction, which changes as a function of location and time and is influenced by many physical systems embedded within it. There are several available estimates of the steady-state global mass, freshwater, and heat transport based on the best available hydrographic data (Talley 2008; Lumpkin and Speer 2007; Ganachaud and Wunsch 2003), as well as a few local estimates of the MOC from one-time full water column hydrographic sections and western boundary arrays (e.g., McDonagh et al. 2008; Kanzow et al. 2008b); however, true time series observations of basin-wide MOC transports are logistically very challenging to collect.

Presently, observing systems capable of quantifying changes in the MOC are at fledgling stages, and most existing systems at best observe only one component (e.g., a specific current or ocean layer) of the global MOC at discrete locations. Long-time series necessary for fully capturing the MOC variability and hence understanding the variations do not yet exist for the global MOC. As such, estimates of the state of the MOC must be inferred from time series of the complete MOC at one particular location (e.g., at 26°N in the Atlantic; Cunningham et al. 2007; Kanzow et al. 2007; Johns et al. 2008), through individual components of the MOC, or from indirect measurements influenced by the strength of the MOC, such

as deep property fields like temperature or salinity.

The only observing system currently in place that measures the MOC spans the subtropical gyre in the North Atlantic near 26°N since April 2004 (called the RAPID Climate Change Program by the U.K. contributors and the MOCHA by the U.S. contributors; see Kanzow et al. 2008a); hence this note concentrates on those observations. During the first year of this new MOC monitoring array, the mean MOC transport was 19.1 Sv² with a standard deviation of 5.6 Sv (Kanzow et al. 2007; Cunningham et al. 2007). Observations of the strength of the MOC

from this array are available only with a time delay as the moorings are recovered over 12- to 18-month intervals. The MOC can be divided into three components: the northward western boundary Florida Current, the wind-driven Ekman transport, and the southward “interior” transport (0–1,000 m deep geostrophic flow between the Bahamas and Africa). Recently, Kanzow et al. (2009) extended the analysis of the interior transport time series through October 2007 (Fig. 3.18). As with the results from the first year of this array, the time series indicates a surprising amount of variability at a range of time scales, including the emergence of a possible annual cycle that looks similar to the annual cycle postulated on the basis of all available section data in Baringer and Molinari (1999). Of note is that all the interior transport values estimated from five repeated CTD³ sections by Bryden et al. (2005) can be found within the seasonal range of the interior transport time series (Fig. 3.18). These results do not disprove the presence of a long-term trend in the strength of the MOC (e.g., as suggested by Bryden et al. 2005; Wunsch and Heimbach 2006), but they do suggest a careful error analysis must be performed that includes the impact of the

² Sv is a Sverdrup or 10⁶ m³/s, a unit commonly used for ocean volume transports.

³ CTD sensors are used to obtain vertical profiles of temperature, salinity, and density in the ocean.

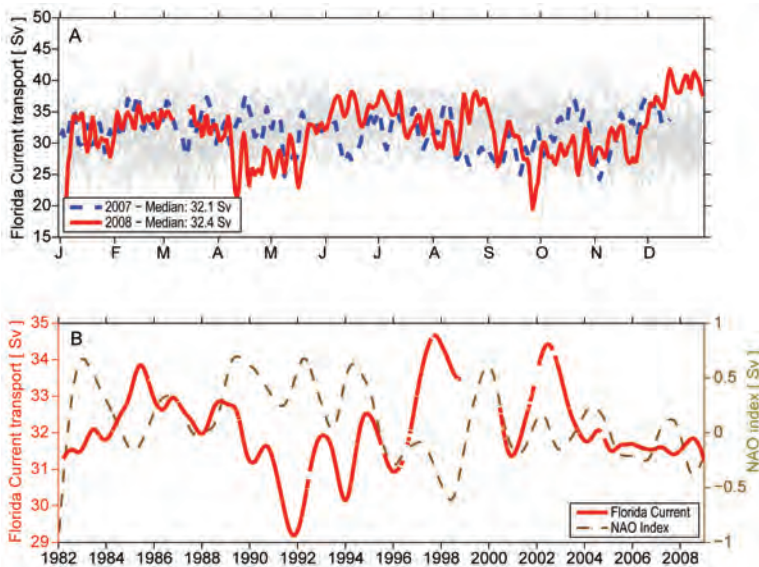


FIG. 3.19. (a) Daily estimates of the transport of the Florida Current for 2008 (red solid line) compared to 2007 (dashed blue line). The daily values of the Florida Current transport for other years since 1982 are shown in light gray. The median transport in 2008 increased slightly relative to 2007 and 2006 and is slightly above the long-term median for the Florida Current (32.2 Sv). (b) Two-year smoothed Florida Current transport (red) and NAO index (dashed orange). The daily Florida Current transport values are accurate to 1.1–1.7 Sv (Meinen et al. 2009, manuscript submitted to *J. Geophys. Res.*) and the smoothed transport to 0.25 Sv (a priori estimate using the observed 3–10-day independent time scale).

underlying higher-frequency variability of the MOC on trend estimates (e.g., Baehr et al. 2008; Baehr et al. 2007; Brennan et al. 2008). Other related studies of the MOC trend are so far contradictory, with some reporting a decrease in the MOC or components of the MOC (e.g., Wunsch and Heimbach 2006; Koltermann et al. 1999; H. R. Longworth et al. 2008, unpublished manuscript), while others suggest no change or even an increase (e.g., Kohl and Stammer 2008; Zhang 2008; Olsen et al. 2008; Lumpkin et al. 2008; Schott et al. 2006). Clearly, while disagreement remains over the details of findings from any particular observing system (e.g., Kanzow et al. 2009), agreement exists that longer time series at multiple locations, particularly of the deep transport components, are needed (e.g., Wunsch 2008).

The longest transport time series of an ocean circulation feature directly linked to the MOC exists at 27°N in the Atlantic, where the bulk of the warm upper limb of the Atlantic MOC is thought to be carried in the Florida Current through the Straits of Florida and the majority of the cold lower limb is believed to be carried to the south in the DWBC just east of the Bahamas (e.g., Meinen et al. 2009, manuscript sub-

mitted to *J. Geophys. Res.*; Baringer and Larsen 2001). Since 1982, variations in the upper limb of the Atlantic MOC have been monitored by measuring the Florida Current transport using a submarine cable across the Straits of Florida in combination with regular hydrographic sections. In 2008 the median transport through the Straits of Florida was 32.4 Sv, well within the middle range of mean annual values (32.2 Sv median transport of the Straits of Florida from 1982 to 2008 with 50% of the annual means within ± 2.2 Sv). There were, however, several unusual high-frequency events during the year (Fig. 3.19): three anomalously low (outside of 2–3 standard deviations of the daily averaged values) transport events during 4–6 January, 7 April–17 May, and 24–29 September, with values as low as about 20 Sv, and an unusually high transport 10–31 December, with values as high as about 42 Sv. Because these events were relatively short lived, it is likely they are local responses to upstream atmospheric forcing and coastally trapped wave processes and are not particularly indicative of a climatically important shift (e.g., Mooers et al. 2005).

Interannual fluctuations in the Florida Current show a negative correlation ($r \sim 0.6$) with the NAO during the 1982–98 time period (Baringer and Larsen 2001); however, while the NAO has been tending to decrease over the past 20 years, the Florida Current transport shows no corresponding long-term trend through 2008 (Meinen et al. 2009, manuscript submitted to *J. Geophys. Res.*; Peng et al. 2009; Beal et al. 2008).

Trends in the global MOC can also be determined through proxies of the MOC strength, such as paleo observations (e.g., Carlson et al. 2008), tracers (e.g., LeBel et al. 2008), and characteristic water masses (e.g., Lohmann et al. 2008; Hawkins and Sutton 2007). For example, during the past year, temperature and salinity observations in the Labrador Sea showed an abrupt return of deep convection between 2007 and 2008 (Våge 2009). Yashayaev and Yoder (2009) showed that the enhanced deep convection in the Labrador Sea in the winter of 2008 was the deepest since 1994 and included the largest heat loss from the ocean to the atmosphere since the mid-1990s, exceeding the long-term mean by 50% (see also Fig. 3.8b). Such anomalous local events may be a precursor to changes in the MOC

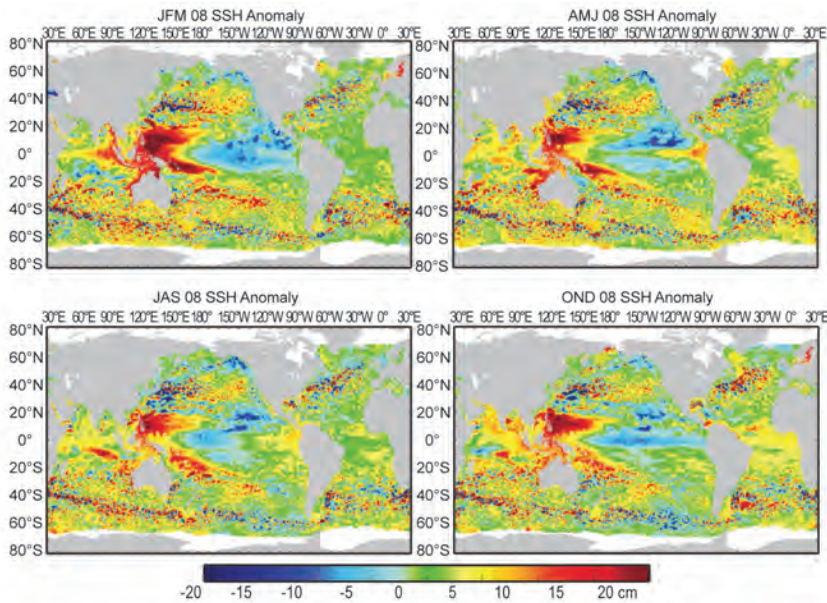


FIG. 3.20. Seasonal SSH anomalies for 2008 relative to the 1993–2007 baseline average are obtained using the multimission gridded sea surface height altimeter product produced by Ssalto/Duacs and distributed by Aviso, with support from CNES (www.aviso.oceanobs.com).

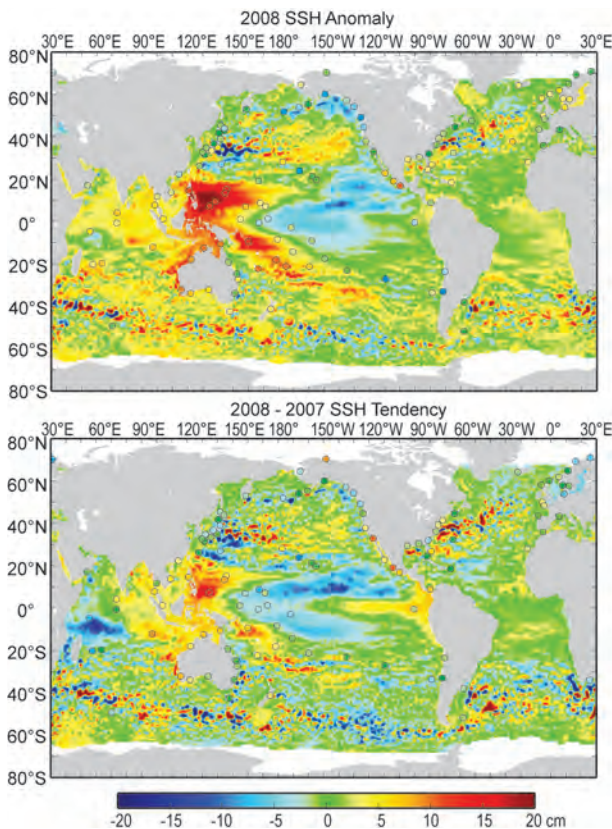


FIG. 3.21. (top) The 2008 SSH anomaly (Ssalto/Duacs product) from the 1993–2007 baseline is compared to the 2008 anomaly computed for tide gauge data (dots) obtained from the University of Hawaii Sea Level Center (<http://uhslc.soest.hawaii.edu/>). (bottom) The difference between 2008 and 2007 annual means.

strength (e.g., Lohmann et al. 2009; Bellucci et al. 2008).

While the MOC is often discussed in terms of the large-scale, full-depth circulation in the North Atlantic Ocean, surface water also sinks into the abyssal ocean around Antarctica (e.g., Orsi et al. 1999). The Antarctic and North Atlantic limbs of the MOC appear to be of similar magnitude (e.g., Lumpkin and Speer 2007), and the Antarctic Bottom Water fills more of the deepest parts of the global ocean than does the North Atlantic Deep Water (e.g., Johnson 2008b). Comparisons of deep hydrographic observations with respect to earlier data reveal some interesting changes associated with Antarctic Bottom Water. For instance, bottom waters of Antarctic origin

in the deep South Atlantic (e.g., Johnson and Doney 2006), Pacific (e.g., Fukasawa et al. 2004; Kawano et al. 2006; Johnson et al. 2007), and south Indian Oceans (e.g., Johnson et al. 2008a) have all warmed over the last decade, indicating a change in the Antarctic contribution to the MOC. Furthermore, bottom waters close to Antarctica, at least in the Indian Ocean sector, also appear to have freshened (Rintoul 2007; Johnson et al. 2008a), consistent with decadal time scale freshening in the source regions for this bottom water (Jacobs et al. 2002). Finally, there are suggestions in both the North Atlantic (Johnson et al. 2008b) and North Pacific (Kouketsu et al. 2009) that the MOC associated with Antarctic Bottom Water may have slowed. Above the bottom water, Argo float data document a large-scale warming and freshening around Antarctica, but there is no accompanying change in horizontal gradients and hence no suggestion of a response to the large-scale increases in westerly winds that have been observed and are projected to continue under a warming climate (e.g., Boning et al. 2008).

i. Sea level variations, 2008 annual assessment—M. A. Merrifield, R. S. Nerem, G. T. Mitchum, L. Miller, E. Leuliette, S. Gill, and P. L. Woodworth

Sea level variations in 2008 are strongly influenced by the persistent, but apparently weakening, La Niña event. We will begin with a description of the associated quarterly sea level anomalies, turning then to

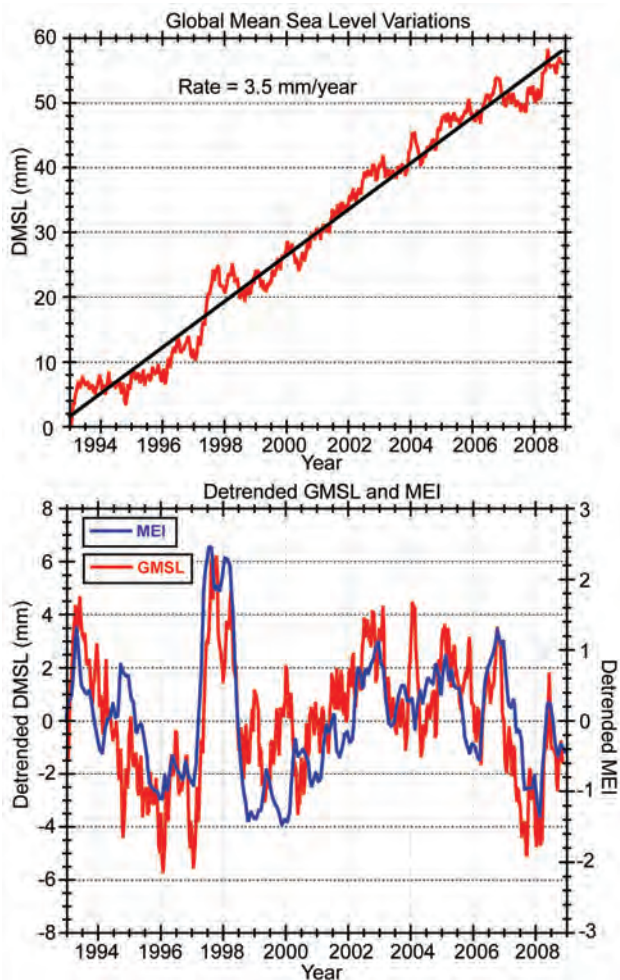


FIG. 3.22. (top) Monthly GMSL (seasonal cycle removed) relative to a linear trend of 3.5 mm yr^{-1} . (bottom) Monthly GMSL (linear trend removed, red) versus the MEI (blue). SSH data provided by the NASA PO.DAAC at the Jet Propulsion Laboratory/California Institute of Technology (<http://podaac.jpl.nasa.gov/>).

the mean of 2008 relative to a long-term mean, and then relative to the 2007 mean, the latter difference being interpreted as the present sea level tendency. We will conclude with an evaluation of global sea level changes in the context of the recent La Niña conditions, and a brief description of sea level extremes observed at tide gauges in 2008.

The La Niña event that developed during 2007 persisted during 2008 with strong positive anomalies in the western tropical Pacific (Fig. 3.20). During JFM 2008 positive SSH anomalies extended throughout the Indonesian Archipelago into the tropical Indian Ocean and southward along the west coast of Australia. The La Niña weakened noticeably during AMJ 2008 with the arrival of a Kelvin wave in the eastern equatorial Pacific.

The annual mean SSH (Fig. 3.21, top) depicts the dominant La Niña state in the Pacific, and the negative-phase PDO pattern in the North Pacific with negative anomalies along the west coast of North America and positive anomalies in the central North Pacific. The shift to a negative PDO began in late 2007. In general, sea level appears to be higher in most regions relative to the 1993–2002 baseline, with the exception of the mid- to high-latitude North Pacific and North Atlantic. The coastal tide gauge and adjacent SSH deviations are similar at most stations.

The SSH tendency (Fig. 3.21, bottom), measured as the difference in annual mean SSH between 2008 and 2007, shows a net increase in sea level in the warm-pool region despite the weakened state of the La Niña during the Kelvin wave event (AMJ; Fig. 3.20). The SSH increase in this region is associated with zonal wind anomalies directed toward the Indonesian Archipelago from both the Indian and Pacific Oceans. A decrease in sea level occurs in the central equatorial

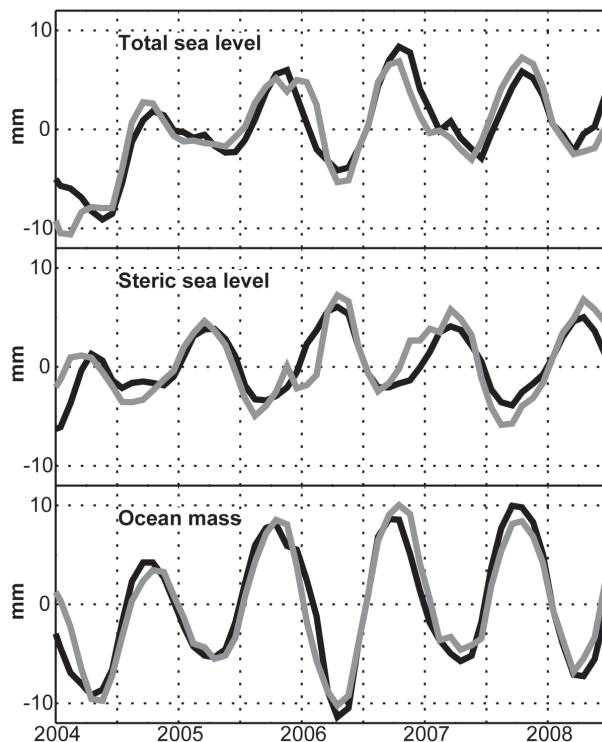


FIG. 3.23. Time series of GMSL, or total sea level, is compared with the two principal components of sea level change, upper-ocean steric change from Argo measurements, and mass change from GRACE measurements (Leuliette and Miller 2009). In this figure, black lines show the observed values and gray lines the inferred values from the complementary observations (e.g., the inferred steric sea level is obtained from observed total sea level–observed ocean mass).

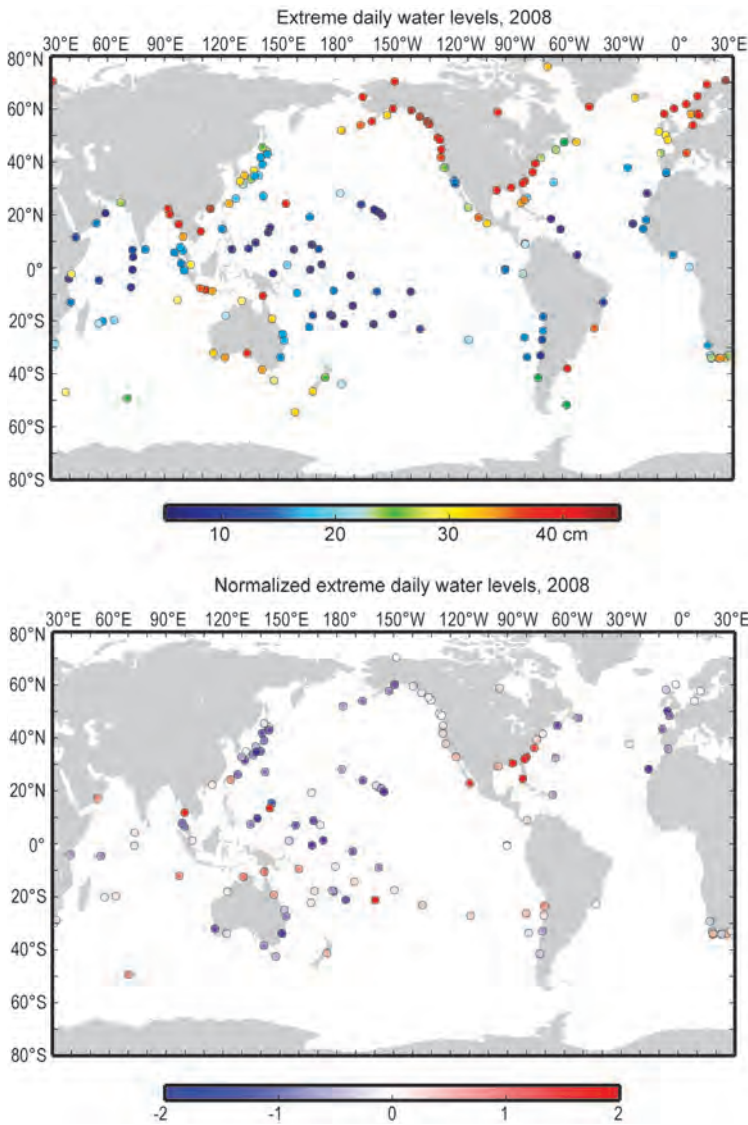


FIG. 3.24. (top) Extreme sea level variability is characterized using the average of the top 2% mean daily sea levels during 2008 relative to the annual mean at each station. (bottom) The extreme values are normalized by subtracting the mean and dividing by the std dev of past-year extreme values for stations with at least 15-yr record lengths.

Pacific and in the eastern tropical Pacific. There is, however, a positive anomaly along Central and South American coasts associated with the Kelvin wave. A strong positive anomaly that occurred during 2007 in the western Indian Ocean fell sharply in 2008, and this region is now substantially below normal. SSH changes in the Atlantic Ocean were weak compared to other regions.

The La Niña event of 2007–08 affected not only regional sea level anomalies but GMSL as well. GMSL has been persistently low during the La Niña event relative to a linear trend of approximately 3.5

$\pm 0.4 \text{ mm yr}^{-1}$ (Fig. 3.22.) (R. S. Nerem et al. 2009, unpublished manuscript). The correspondence between GMSL and the MEI (www.cdc.noaa.gov/people/klaus.wolter/MEI/mei.html) shows that El Niño and La Niña events have a strong influence on global sea level. Once this interannual variability is accounted for, the inferred rate of GMSL change remains remarkably constant, suggesting that La Niña may partially explain the flattening of the GMSL curve over the past one to two years.

Variations in GMSL due to changes in ocean density (steric sea level) and ocean mass are currently under investigation using satellite altimeters, the Argo array (ocean thermal), and the GRACE time series (ice melt and other hydrological variations), and preliminary investigations are beginning to document these changes (e.g., Willis et al. 2008; Leuliette and Miller 2009). On seasonal time scales (Fig. 3.23), the steric and mass components of GMSL are 180° out of phase due to differences in continental surface area in the Northern and Southern Hemispheres, which leads to asymmetries in net ocean heat flux and river runoff (Willis et al. 2008). These analyses of seasonal variations demonstrate the power of the present system for observing and interpreting sea level variations. As the time series from Argo and GRACE lengthen, the contributions to interannual GMSL change will become increasingly clear.

Extreme sea level variability during 2008 is examined using daily averages obtained from a global set of tide gauges (Fig. 3.24). Extreme sea levels, taken as the average of the 2% highest daily values relative to the annual mean level (top), were high along the coasts of North America, Europe, and Southeast Asia, and low at most of the islands in the tropics. For time series with at least 15 years of record length, we normalize the levels by removing the mean and dividing by the standard deviation of extreme sea levels for all available years (Fig. 3.24, bottom). By this measure, extremes along the southeast coast and Gulf Coast of the United States were notably higher than normal. Other areas of unusually high values include northern Australia and isolated stations south of the

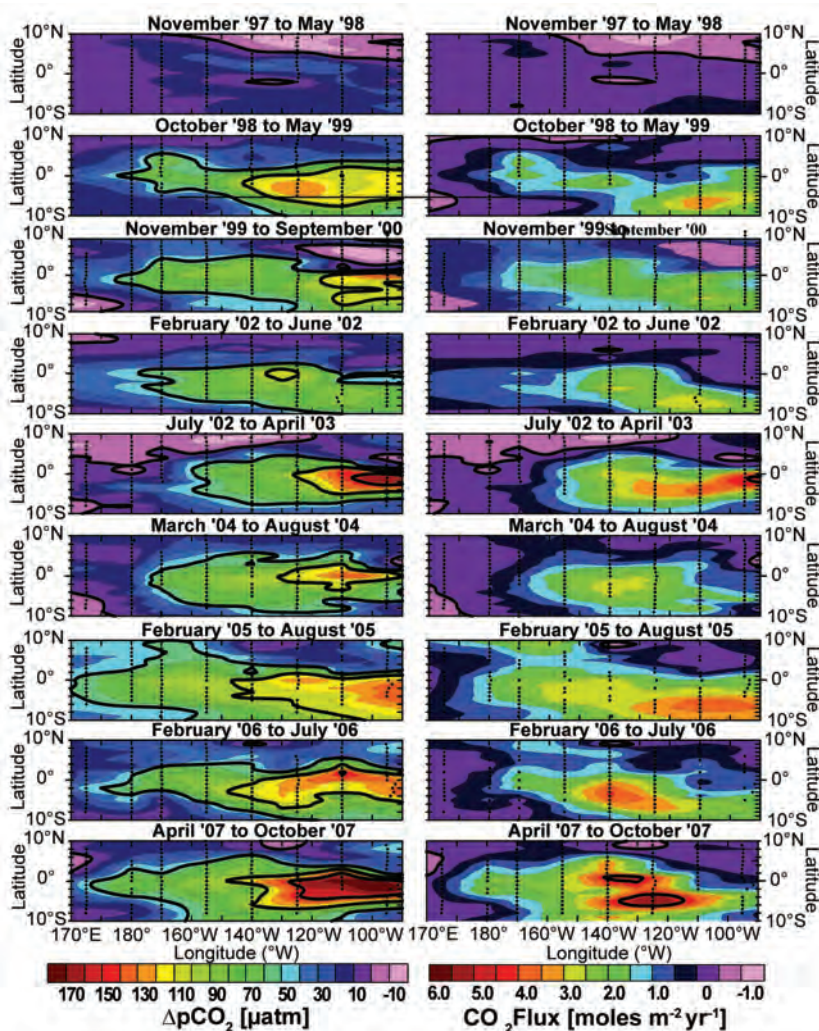


FIG. 3.25. Plots of sea-air $p\text{CO}_2$ difference and air-sea CO_2 flux in the equatorial Pacific between 1997 and 2007 based on underway CO_2 measurements collected on the TAO service cruises. The nominal cruise track lines are shown in black. A complete survey of the region is completed approximately every six months. The black and dark purple areas indicate where the atmosphere and seawater $p\text{CO}_2$ values are nearly balanced. The pink areas indicate ocean uptake of CO_2 , and the blue to red colors indicate areas of ocean CO_2 out-gassing.

equator in the tropical Pacific. Extremes in Europe, Japan, and South Australia, and at island stations in the equatorial Pacific, were well below normal.

j. The global ocean carbon cycle—C. L. Sabine, R. A. Feely, R. Wanninkhof, and T. Takahashi

1) AIR-SEA CARBON DIOXIDE FLUXES

The time and space scales of variability in the air-sea CO_2 flux make it challenging to assess global fluxes based on in situ surface observations. The latest global flux map is based on approximately 3 million measurements collected between 1970 and 2007 (Takahashi et al. 2009). The annual mean con-

temporary CO_2 flux over the global oceans in 2000 is estimated to be a net uptake of $1.4 \pm 0.7 \text{ Pg-C yr}^{-1}$. As with the previous maps, the estimate is for a “normal” year when there are no significant El Niño signals in the equatorial Pacific. Because the loss of CO_2 from the equatorial Pacific to the atmosphere is depressed during El Niños (Feely et al. 2006), these conditions result in a net increase in the global ocean CO_2 uptake for that year. Seasonal-to-annual estimates of net air-sea CO_2 fluxes are needed to better understand the changing role of the ocean in the global carbon cycle. The updated empirical approach to quantifying the air-sea CO_2 exchange utilizing in situ, climatological, and satellite data is described in Sabine et al. (2008). The diverse data streams and lags in availability of quality-controlled atmospheric CO_2 , satellite, and assimilation products preclude real-time analysis such that quarterly air-sea CO_2 flux maps are only available for the period from 1983 to 2007. The global mean air-sea CO_2 flux for this period, including the ENSO effects, gives an average uptake of $1.74 \text{ Pg-C yr}^{-1}$. Assuming the preindustrial steady-state ocean was a source of 0.4 Pg-C yr^{-1} (Jacobson et al. 2007), the estimated average flux equates to a net ocean anthropogenic CO_2 uptake of $2.14 \text{ Pg-C yr}^{-1}$. This is consistent with the oceanic anthropogenic

CO_2 sink estimate of $2.2 \pm 0.5 \text{ Pg-C yr}^{-1}$ from Bindoff et al. (2007), based on several different approaches. Gruber et al. (2009) analyzed the oceanic uptake rates of anthropogenic CO_2 for the period of 1990 to early 2000, which were estimated from observations (sea-air $p\text{CO}_2$ difference, sea-air ^{13}C disequilibrium, and atmospheric O_2/N_2) and general circulation models (ocean data inversion, atmospheric data inversion, and ocean biogeochemical models). Multiple techniques for estimating ocean anthropogenic CO_2 , including observational approaches, numerical models, and techniques that blend observations and models, were found to be mutually consistent within their respec-

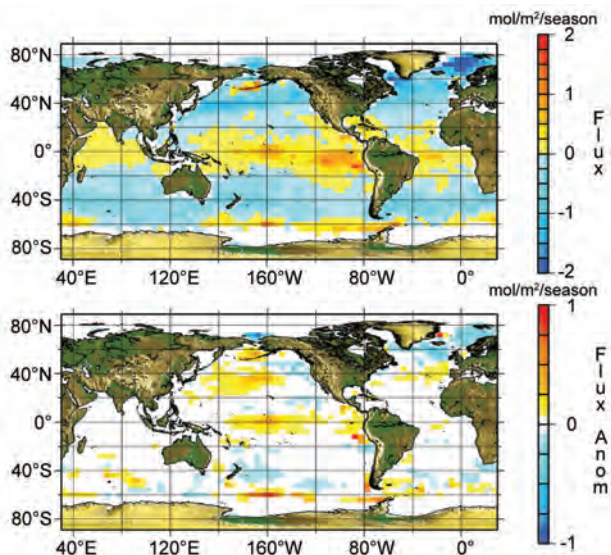


FIG. 3.26. Maps of (a) net air–sea CO₂ fluxes and (b) air–sea CO₂ flux anomaly for Sep–Dec 2007. Coastal pixels and those with ice cover are masked in gray. Negative fluxes represent uptake of CO₂ by the ocean. Output and graphic provided by J. Trinanes.

tive uncertainties, ranging from 1.5 ± 0.9 Pg-C yr⁻¹ to 2.4 ± 0.5 Pg-C yr⁻¹ (Gruber et al. 2009).

Figure 3.25 shows the measured sea–air CO₂ differences and net fluxes in the equatorial Pacific for a 10-yr period from 1997 to 2007. The top, from the fall of 1997 and spring of 1998, shows the very low out-gassing conditions of the 1997/98 El Niño. This is in contrast to the bottom, which shows very strong out-gassing during the 2007 La Niña shown by the Multivariate ENSO Index (www.cdc.noaa.gov/enso/enso.mei_index.html). The difference in the estimated flux between the top (November 1997–May 1998) and the bottom panels (April 2007–October 2007) is 0.39 Pg-C, or about 20% of the long-term average annual global air–sea CO₂ flux.

The global pattern of the net air–sea CO₂ flux for October–December 2007 is presented in Fig. 3.26a based on seasonal correlations between sea surface temperature and pCO₂ for each 4° by 5° pixel of the Takahashi et al. (2009) map (see Lee et al. 1998; Park et al. 2006; and Sabine et al. 2008 for methods). The interannual variability in air–sea CO₂ fluxes is determined from these relationships and global interannual sea surface temperature and wind speed anomalies derived from satellite and assimilation products. It shows the characteristic global pattern of net release of CO₂ in the tropics and regions of upwelling and CO₂ uptake in the mid- and high latitudes. Of note are the regions of efflux near the Antarctic ice edge that partially offset the sink strength of the Southern

Ocean. Figure 3.26b shows the difference between the September–December 2007 air–sea fluxes and the average September–December flux pattern for the whole record (1983–2007). The large positive anomaly in the equatorial Pacific means that there was enhanced out-gassing of CO₂ consistent with the measurements shown in the bottom of Fig. 3.25. These estimates suggest the La Niña effect impacted a much larger area of the Pacific than the region measured from the cruises to service the TAO moorings. Very strong positive local anomalies are determined off the coast of Peru associated with intensified upwelling and stronger winds. Positive anomalies are also estimated for the subtropical North Pacific. The cause of the North Pacific anomaly, and to a lesser extent in the North Atlantic, is being validated and is under investigation. Observations from volunteer observing ships in the North Atlantic suggest that this is an actual anomaly rather than an artifact of the approach. It is a continuation of the depressed North Atlantic CO₂ sink in this region, albeit of lesser magnitude than that observed in the mid-1990s (Schuster and Watson 2007). Due to changing shipping routes there were no measurements in that region of the North Pacific to validate the results for the North Pacific, but the strong positive air–sea CO₂ flux anomaly off the coast of Peru was confirmed with measurements from the flux reference buoy deployed as part of the VOCALS (www.eol.ucar.edu/projects/vocals/) project and ship-based observations from NOAA ship R/V *Ronald H. Brown* servicing the buoy.

A negative correlation ($r^2 \sim 0.6$) between the Multivariate ENSO Index and global air–sea CO₂ fluxes is observed in the long-term flux record. Positive MEI indicates El Niño conditions and low CO₂ out-gassing. The boreal winter of 2007 showed a negative MEI (< -1) corresponding to an increased equatorial Pacific CO₂ flux to the atmosphere, or depressed net global oceanic uptake of CO₂ (Fig. 3.26b). The global mean CO₂ uptake for 2007 is estimated at 1.67 Pg-C, about 0.07 Pg-C lower than the long-term average. This seasonal anomaly is the third-largest determined with this method since 1983. The low global uptake is attributed, in large part, to the La Niña that was observed in the equatorial Pacific at that time. It intensified toward the end of 2007 as observed with sea surface temperature observations (Reynolds and Xue 2008).

2) SUBSURFACE CARBON INVENTORY

In 2003, the U.S. CLIVAR/CO₂ Repeat Hydrography Program began reoccupying a subset of lines from the WOCE/JGOFS global ocean survey con-

ducted in the 1990s. The program has identified 19 hydrographic sections distributed around the global ocean that will be surveyed approximately every 10 years to examine changes in ocean carbon and other physical and biogeochemical tracers. In 2008 two lines were completed: I6S in the southwestern Indian Ocean, nominally along 30°E, and P18 in the southeastern Pacific, nominally along 105°W.

Figure 3.27 shows sections of DIC along P18 in 2008 and 1994. To first order the distributions look similar for both years, but the difference plot (Fig. 3.27, bottom) shows patchy increases as large as 50 $\mu\text{mol kg}^{-1}$. This patchy pattern does not simply reflect a secular increase in CO_2 but is also influenced by variability in the natural carbon distributions at interannual and shorter time scales. Aliasing from mesoscale eddies and frontal oscillations that displace isopycnal surfaces (Haine and Gray 2001; Peacock et al. 2005), as well as variations in water mass properties associated with climate modes such as the El Niño–Southern Oscillation (Feely et al. 2002), can be significant when comparing two cruises separated in time.

To correct for these variations and isolate the changes due to uptake of CO_2 from the atmosphere, we use the multiple linear regression approach first introduced by Wallace (1995). The application of these corrections varies depending on data quality and the oceanographic conditions along the section; thus each section must be evaluated separately. A full global assessment of ocean DIC changes cannot be made until the resurvey of the oceans is completed in the next few years. However, each updated ocean section provides incremental insight into how carbon uptake rates are evolving spatially and temporally.

Table 1 summarizes the current best estimates of anthropogenic CO_2 accumulation along representative north–south cruise tracks in the Atlantic, Pacific, and Indian Oceans over the last decade. If these values are representative of the basin averages, then the changes over the last decade are somewhat different from the pattern of long-term accumula-

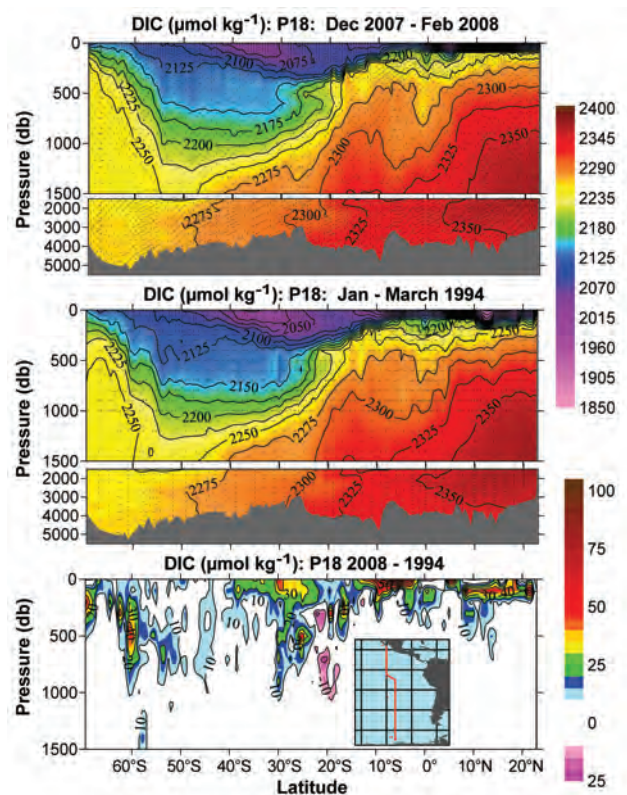


FIG. 3.27. Sections of dissolved inorganic carbon ($\mu\text{mol kg}^{-1}$) nominally along 105°W in (top) 2008 and (middle) 1994. The bottom section shows the DIC change between the two cruises (2008–1994). Black dots show sample locations. Inset map shows cruise track in red.

tion. For example, Sabine et al. (2004) found that the largest accumulation of anthropogenic CO_2 over the last 200 years was in the North Atlantic. This was attributed to the transport of waters rich in anthropogenic CO_2 into the ocean interior by the formation of North Atlantic Deep Water. The repeat hydrography results, however, indicate that over the last decade the North Atlantic has not had the largest increase in anthropogenic carbon storage. This finding is consistent with other independent estimates that the North Atlantic uptake rate has decreased over

TABLE 3.1. Estimates of ocean column inventory changes in anthropogenic carbon ($\text{mol C m}^{-2} \text{yr}^{-1}$) over the last decade.

	Atlantic (25°W) 1993–2005	Pacific (152°W) 1991–2006	Indian (90°E) 1995–2007
Northern Hemisphere	0.63	0.25	0.63
Southern Hemisphere	0.75	0.41	0.83

the last decade (Schuster and Watson 2007; Thomas et al. 2008). The largest increases in anthropogenic carbon accumulation along these sections appear to be in the Southern Hemisphere oceans.

Figure 3.28 shows the change in carbon column inventories between the CLIVAR (2008), WOCE (1995), and GEOSECS (1978) cruises in the eastern Indian Ocean along 90°E. The pattern of average annual carbon increases between 1995 and 2008 were similar to the pattern of increases between 1978 and 1995, but the magnitude of the increases over the last decade are about twice the increases prior to 1995. These findings appear to contradict some recently published model results and surface ocean pCO₂ observations that have suggested that the Southern Ocean uptake of CO₂ has decreased over the last few decades (Le Quéré et al. 2007; Lovenduski et al. 2007; Takahashi et al. 2009). There are still more lines that need to be examined in the Southern Ocean, but these initial results illustrate the importance of studying the linkages and differences between CO₂ uptake from the atmosphere and the ultimate storage of carbon in the ocean interior.

Because atmospheric CO₂ concentrations are growing at a nearly exponential rate, it is not surprising to find that the rate of carbon storage is increasing with time. However, there are two processes that control the rate of anthropogenic carbon increases in the ocean: the equilibration time between the ocean and the atmosphere and the rate at which waters containing anthropogenic carbon are moved into the ocean's interior. In most places the surface ocean CO₂ values are increasing at roughly the same rate as the atmosphere (Takahashi et al. 2009). This means that anthropogenic CO₂ is accumulating in surface waters everywhere at approximately the same rate. There are only a few locations, however, where surface waters are moving into the ocean interior.

North of about 55°S the difference between the two curves in Fig. 3.28 is reasonably consistent. Because both curves show the largest overall accumulations of carbon in the southern subtropical gyre, the percent change in the carbon accumulation rate is much larger north of 10°S (from 0.2–0.3 to ~0.6 mol m⁻² yr⁻¹, or roughly a 100% increase) compared to the region south of approximately 10°S (from 0.7–0.9 to 1.0–1.2 mol m⁻² yr⁻¹, or about a 30% increase). This observation is consistent with the idea that surface layer accumulation of anthropogenic carbon has increased at all latitudes, but the rate of transport of anthropogenic carbon into the ocean interior has not changed dramatically along this section. The anthropogenic carbon penetration is still

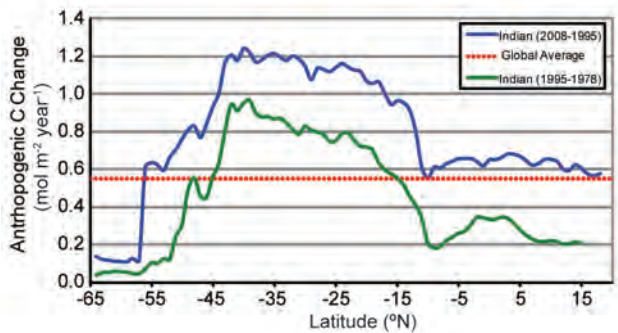


FIG. 3.28. Column Inventory changes as a function of latitude along ~90°E in the eastern Indian Ocean. The blue line is the average annual change between 2007 and 1995. The green line is the average annual change between 1995 and 1978. The red dotted line is the global-average annual uptake of anthropogenic CO₂ divided by the surface area of the ocean.

relatively shallow north of 10°S, thus the increase in surface uptake resulted in a significant increase in the total carbon column inventory. South of 10°S, however, much of the anthropogenic carbon is found in the intermediate waters. An increase in the surface accumulation rate without a subsequent increase in the rate at which CO₂ is moved into the ocean interior, therefore, would result in a smaller percent increase in the total column inventory as observed.

These latest results show conclusively that anthropogenic CO₂ is continuing to accumulate in the Atlantic, Pacific, and Indian Oceans and suggest that the accumulation rates can vary over decadal time scales. However, a single transect through an ocean basin is not sufficient for characterizing the full patterns of anthropogenic CO₂ storage. More in-depth analyses will be undertaken once the global survey is complete. Because circulation and biological processes changes can vary in cycles often associated with ocean climate reorganizations such as ENSO, North Atlantic Oscillation, Pacific decadal oscillation, and southern annular mode, it is critical to continue to monitor the changes in carbon inventories and how they interact with the secular increases in anthropogenic CO₂.

k. Global ocean phytoplankton—M. J. Behrenfeld, D. A. Siegel, R. T. O'Malley, and S. Maritorena

Photosynthesis by the free-floating, single-celled phytoplankton of the upper sunlit “photic” layer of the global ocean is the overwhelmingly dominant source of organic matter fueling marine ecosystems. Phytoplankton contribute roughly half of annual biospheric (i.e., terrestrial and aquatic) NPP (gross photosynthesis minus plant respiration), and their

NEW EVIDENCE FOR OCEAN ACIDIFICATION IN COASTAL WATERS OF NORTH AMERICA—R. A. FEELY AND A. G. DICKSON

Over the past two centuries the release of CO_2 from humankind's combined industrial and agricultural practices has resulted in atmospheric CO_2 concentrations that are now higher than experienced on the Earth for at least the last 800,000 years (Lüthi et al. 2008). During this period the oceans have taken up approximately one-third of the total amount of CO_2 produced by human activities (Sabine et al. 2004). This addition of anthropogenic CO_2 to the ocean has reduced the surface ocean pH by about 0.1 to date (a process known as ocean acidification) and is expected to reduce pH by a further 0.3 units by the end of this century (Feely et al. 2004). It now appears likely that the level of CO_2 in the atmosphere might double over its preindustrial levels by the middle of this century. This rapid change in ocean chemistry is more dramatic than at any time in the past 20 million years (Feely et al. 2004). This pH decrease will lead to a reduction in the saturation state of seawater with respect to calcite and aragonite, which are the two most common types of calcium carbonate formed by marine organisms (Feely et al. 2004). These changes in seawater chemistry have consequences for a wide variety of marine organisms in coastal and open ocean ecosystems. Many species of marine calcifiers, such as clams, oysters, mussels, sea urchins, and corals, have exhibited reduced calcification rates in response to elevated CO_2 levels (Kleypas et al. 2006; Fabry et al. 2008; Doney et al. 2009). On the other hand, other

noncalcifying species, including sea grasses (Palacios and Zimmermann 2007; Hall-Spencer et al. 2008), and nitrogen-fixing bacteria (Hutchins et al. 2007) appear to produce increased biomass under increased CO_2 levels.

Recent studies have provided new findings that organisms growing in estuaries or in coastal upwelling zones, such as near river mouths or along the continental shelf of the west coast of North America, may already be experiencing significant biological effects resulting from the combined impacts of freshwater input, coastal upwelling, and ocean acidification (Salisbury et al. 2008; Feely et al. 2008). For example, Salisbury et al. (2008) demonstrated

that discharge of acidic river water over the continental shelf may result in poor conditions for shell formation. When the low-alkalinity river water mixes into the surface ocean it can significantly reduce the aragonite or calcite saturation state. For many rivers, this process could inhibit the development of certain shellfish larvae such as the commercially valuable clam *Mya arenaria*.

On the west coast of North America, the seasonal upwelling of subsurface waters along the coast brings CO_2 -enriched waters onto the shelf and, in some instances, into the surface ocean (Fig. 3.29). It appears that this water, in addition to its original high level of CO_2 resulting from natural respiration processes in the subsurface layers, is also significantly contaminated with anthropogenic CO_2 as it was last in contact with the atmosphere about 50 years ago when it took up additional CO_2 from the atmosphere. An immediate consequence of this additional CO_2 is that the CO_2 concentrations in these upwelled waters will be significantly greater than they would have been in preindustrial times. Furthermore, each ensuing year will draw on water that has been exposed to the atmosphere still more recently, resulting in yet higher CO_2 levels. Because these "ocean-acidified" upwelled waters are undersaturated with respect to aragonite, they are already a potential threat to many of the calcifying aragonitic species that live along such coasts.

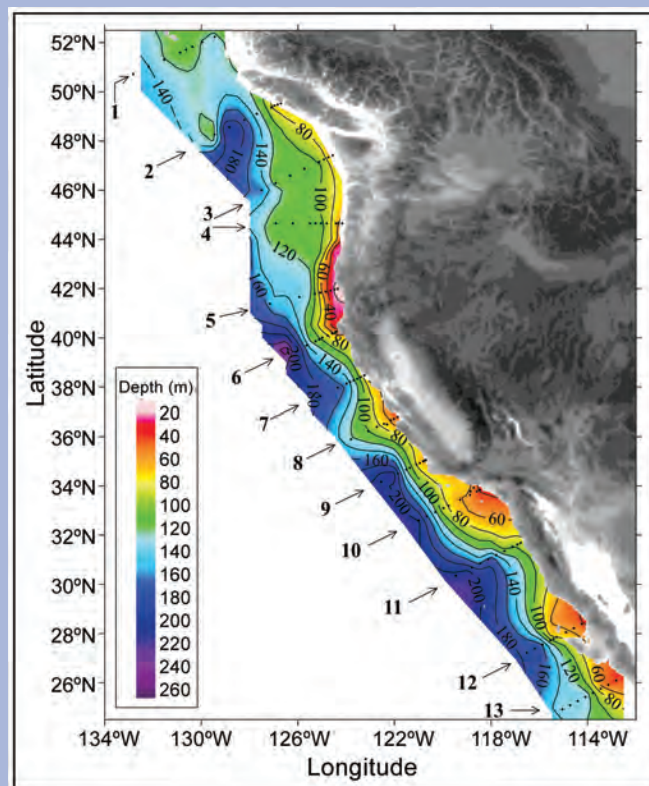


FIG. 3.29 (after Feely et al. 2008). Distribution of the depths of "ocean acidified" undersaturated water (aragonite saturation < 1.0 ; $\text{pH} < 7.75$) on the continental shelf of western North America from Queen Charlotte Sound, Canada, to San Gregorio Baja California Sur, Mexico. On transect line 5, the corrosive water reaches all the way to the surface in the inshore waters near the coast. The black dots represent station locations.

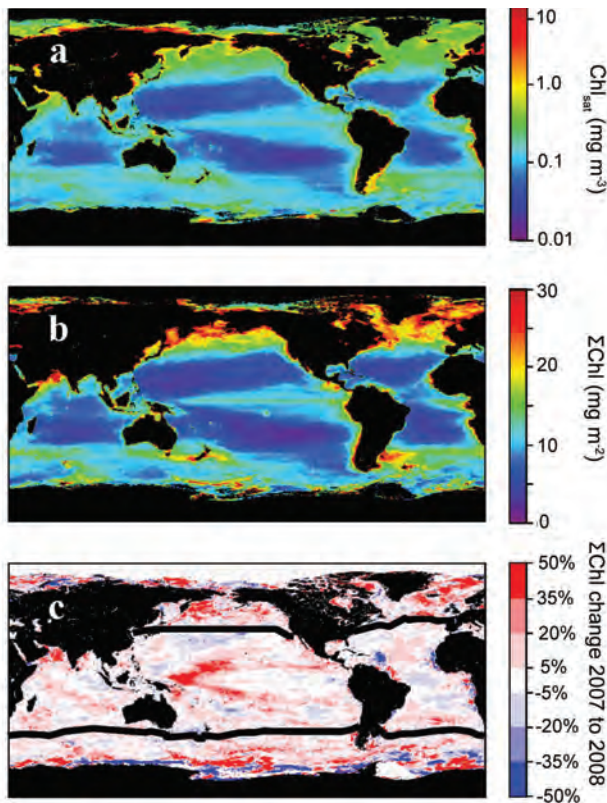


FIG. 3.30. (a) Average MODIS-Aqua Chl_{sat} for 2008. (b) Average MODIS-Aqua ΣChl for 2008. (c) Percentage change in ΣChl from 2007 to 2008. Heavy black lines demark permanently stratified oceans (2007 average SST $>15^{\circ}\text{C}$) from higher-latitude regions (2007 average SST $<15^{\circ}\text{C}$). Because data were only available through day 320 of 2008 at the time of our analysis, here and in the main text annual values are for Julian dates 321 of a given year to 320 of the following year (e.g., the 2008 period = Julian day 321, 2007 to Julian day 320, 2008). Photic zone chlorophyll content calculated following Behrenfeld et al. (2006).

photosynthetic carbon fixation is the primary conduit through which atmospheric CO_2 is transferred into ocean organic carbon pools. Thus, these tiny suspended ocean “plants” play a vital role in world fisheries and the Earth’s biogeochemical cycles.

The productivity of phytoplankton depends on the availability of sunlight, macronutrients (e.g., nitrogen, phosphorous), and micronutrients (e.g., iron), and thus is sensitive to climate-driven changes in these resources. Since 1997, a continuous satellite record of global climate-quality ocean color data has existed, allowing quantification of phytoplankton properties and investigation of broad relationships between upper-ocean environmental conditions and biology (e.g., McClain 2009). The ecosystem property most often derived from ocean color observations is the

surface chlorophyll concentration (Chl_{sat}) (Fig. 3.30a), which can be taken as representative of the upper mixed layer and is a complex expression of phytoplankton standing stock (biomass) and physiological responses to prevailing light and nutrient levels. Chl_{sat} varies globally by three orders of magnitude (roughly 0.03 to $>30 \text{ mg m}^{-3}$). A relevant property for ocean biology and biogeochemistry is the chlorophyll standing stock integrated over the photic zone (ΣChl ; e.g., Behrenfeld et al. 2006), where the photic zone is traditionally defined as the layer between the surface and 1% light depth. Qualitatively, ΣChl exhibits a similar global distribution as Chl_{sat} (Fig. 3.30b), but ΣChl is roughly proportional to the square root of Chl_{sat} , so its value range is constrained to only 1.3 orders of magnitude (Behrenfeld et al. 2008a; Behrenfeld and Falkowski 1997).

Since the beginning of the satellite ocean color record, a striking correspondence has emerged between global variations in ΣChl and SST (Gregg et al. 2005; Behrenfeld et al. 2006). In 2008, our ability to monitor, refine, and interpret this relationship weakened. For the past decade, the SeaWiFS provided an unbroken time series of well-characterized global ocean data, but multiple satellite system failures this past year yielded temporal discontinuities in the record, with data gaps extending several months. Consequently, continuation of the long-term satellite record requires merging SeaWiFS data with products from the MODIS on the *Aqua* EOS satellite, which unavoidably introduces a potential for intersensor artifacts in the time series. Data from the MODIS sensor on the *Terra* EOS satellite are not used because the MODIS-*Terra* sensor has many technical issues that limit its utility for climate applications (e.g., Kwiatkowska et al. 2008).

SeaWiFS and MODIS-*Aqua* observations overlap continuously between July 2002 and December 2007. Over this 66-month period, global-average Chl_{sat} for SeaWiFS is 0.302 mg m^{-3} , average photic zone chlorophyll (ΣChl) is 13.5 mg m^{-2} , and total global chlorophyll standing stock for the photic zone averages 4.6 Tg. Sixty-one percent of this global chlorophyll stock is found in the permanently stratified oceans (approximated here as waters with annual average SST in 2007 of $>15^{\circ}\text{C}$), which cover 72% of the ocean surface. The remaining 39% of global chlorophyll stock is found in the more productive seasonal seas at higher latitudes. By comparison, MODIS-*Aqua* data for the same 66-month period give a global-average Chl_{sat} of 0.266 mg m^{-3} , an average ΣChl of 12.1 mg m^{-2} , and an average global chlorophyll stock of 4.1 Tg, with 62% of this stock found in the

permanently stratified oceans. The elevated values of chlorophyll for SeaWiFS relative to MODIS-*Aqua* reflect a persistent bias between the two datasets, as clearly seen in the time series of monthly chlorophyll stocks for the permanently stratified oceans (Fig. 3.31a). On average, SeaWiFS chlorophyll values are 13.2% higher than MODIS-*Aqua*. When applied to the Vertically Generalized Production Model (Behrenfeld and Falkowski 1997), SeaWiFS data yield annual ocean NPP estimates ranging from 51.2 to 52.3 Pg C y^{-1} , while MODIS-*Aqua* gives values of 45.6 to 46.9 Pg C y^{-1} (average intersensor bias between NPP values is 12.3%).

Sensor gains for SeaWiFS and MODIS-*Aqua* are determined through comparison with the same in situ dataset (e.g., Franz et al. 2007), but no deliberate effort has been specifically made to date to minimize discrepancies between the resulting satellite data products. In 2009, both datasets will undergo a complete reprocessing, after which issues of bias between the two sensors should be reevaluated.

For 2008, the complete annual record provided by MODIS-*Aqua* gives an average Chl_{sat} of 0.271 mg m^{-3} and an average ΣChl of 12.4 mg m^{-2} . While the MODIS-*Aqua* globally integrated chlorophyll standing stock for 2008 of 4.1 Tg is only 1.4% higher than the 2007 value, regional changes in ΣChl were substantial and ranged to $\pm 50\%$ (Fig. 3.30c). Pixel-level comparison of these ΣChl changes with coincident changes in MODIS-*Aqua* SST data yields an inverse relationship for 66% of the stratified ocean (i.e., ΣChl decreases with increasing SST, and vice versa), while only 34% of the region exhibits a positive correlation. This result can be viewed in the broader context of the full satellite record by merging SeaWiFS, MODIS-*Aqua*, and AVHRR data and comparing monthly chlorophyll and SST anomalies for the permanently stratified, northern high-latitude, and southern high-latitude zones.

Monthly chlorophyll anomalies for the stratified oceans exhibit a remarkable coherence between the two records ($r^2 = 0.81$) (Fig. 3.31b), despite the bias between SeaWiFS and MODIS-*Aqua* data (e.g., Fig. 3.31a). Similar intersensor agreement in chlorophyll anomalies is also found for the two high-latitude zones (i.e., annual average SST $< 15^\circ C$). While these results do not diminish the impact of SeaWiFS/MODIS-*Aqua* biases on quantitative analyses of phytoplankton standing stocks and rates, they do imply that anomaly trends can be evaluated across the merged dataset. With respect to SST and in contrast to chlorophyll, AVHRR and MODIS-*Aqua* data for the 2002–07 period do not show significant intersensor

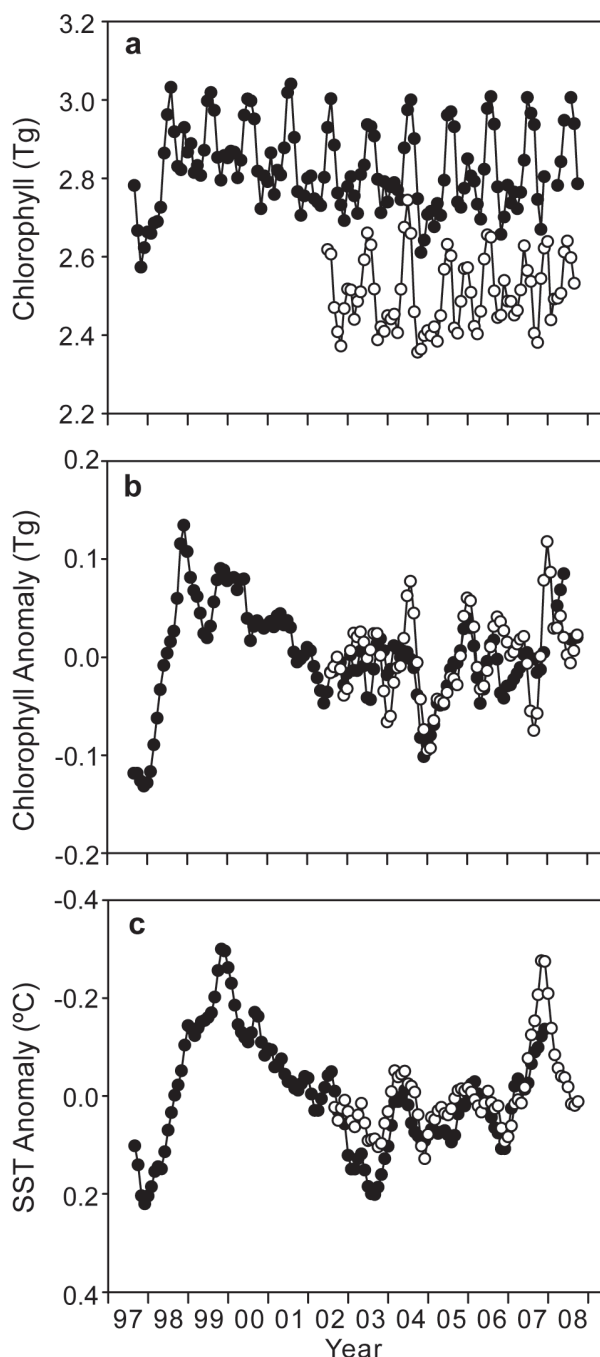


FIG. 3.31. (a) Monthly photic zone chlorophyll concentrations (= average ΣChl times area) for the permanently stratified oceans (SST $> 15^\circ C$; Fig. 1c). Solid symbols are SeaWiFS data. Open symbols are MODIS-*Aqua* data. (b) Monthly anomalies in stratified ocean photic zone chlorophyll for SeaWiFS (solid symbols) and MODIS-*Aqua* (open symbols). Anomalies represent the difference between photic zone chlorophyll for a given month and the average value for that month for a given sensor record. (c) Monthly anomalies in mean SST for the stratified oceans based on AVHRR-quality 5–8 data (solid symbols) and MODIS SST4 data (open symbols).

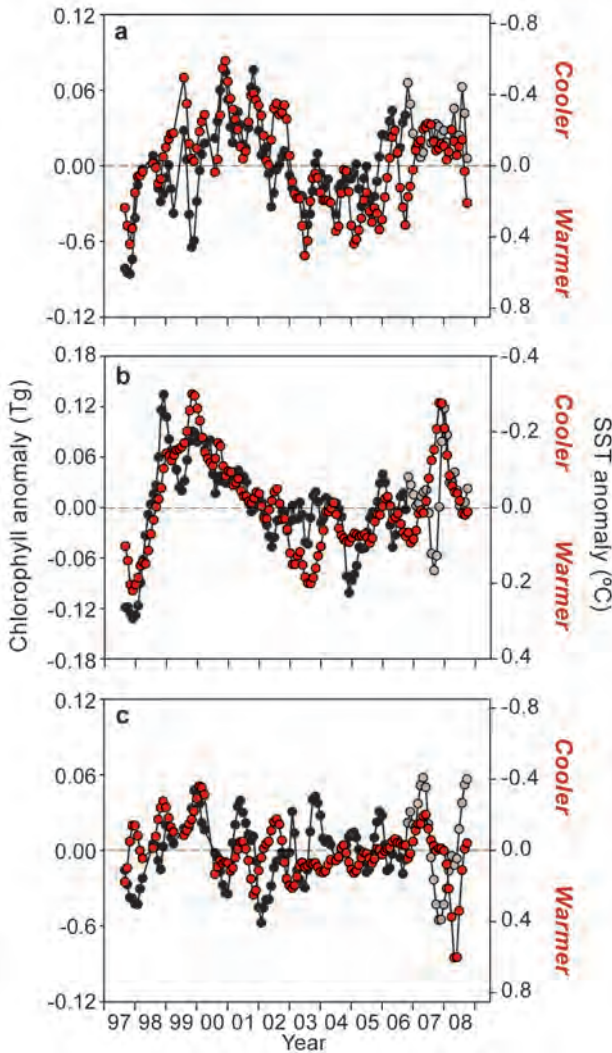


FIG. 3.32. Comparison of monthly anomalies in photic zone chlorophyll (black and gray symbols, left axis) and SST (red symbols, right axis). (a) Northern waters with 2007 average SST < 15°C. (b) Permanently stratified waters with 2007 average SST > 15°C. (c) Southern waters with 2007 average SST < 15°C. (a–c) Solid black symbols are SeaWiFS data. Gray symbols are MODIS–Aqua data. MODIS–Aqua data are spliced into the SeaWiFS record beginning on Julian day 321, 2006, to be consistent with Fig. 1. Horizontal dashed line in each panel corresponds to monthly climatological average values. (Note, left axes increase from bottom to top, while right axes decrease from bottom to top.)

biases and their SST anomalies are highly correlated ($r^2 = 0.91$) (Fig. 3.31c).

From the merged datasets, we find that the chlorophyll–SST relationship observed during 2008 is consistent with longer-term patterns observed since the first SeaWiFS images in September 1997 (Fig. 3.32). At northern high latitudes, oscillations in monthly chlorophyll anomalies are inversely cor-

related with SST anomalies (linear regression slope $p < 0.01$) (Fig. 3.32a). Note that the SST anomaly scale in all panels of Fig. 3.32 is the right-hand axes, with cooling at the top and warming at the bottom (as in Fig. 3.31c). Similarly, chlorophyll and SST anomalies are inversely related in the permanently stratified oceans (linear regression slope $p < 0.001$) (Fig. 3.32b). At high southern latitudes, weaker temporal trends in chlorophyll and SST are found, but an inverse relationship is still apparent and significant (linear regression slope $p < 0.05$). Combining the two polar regions, we find that the slope of the chlorophyll–SST relationship is a factor of 3 steeper (i.e., greater change in chlorophyll per unit change in SST) than in the permanently stratified zone.

Despite all three of our global zones exhibiting inverse chlorophyll–SST relationships, it is important to recognize their correlative, not causative, underpinnings. Ninety percent of the SST anomalies shown in Fig. 3.32 are within $\pm 0.3^\circ\text{C}$ of the 11-yr record monthly mean values (s.d. = 0.11°C), and the full range of anomaly values barely span a 1°C range. The direct physiological consequences (e.g., enzymatic reaction rates) of such minute temperature changes are negligible. Thus, correlations between SST and chlorophyll anomalies emerge because SST acts as a surrogate for other environmental factors that vary with SST and directly impact phytoplankton chlorophyll levels. Two such factors are nutrients (including iron) and mixed layer light levels. In general, surface layer warming is associated with stronger surface layer stratification and shallower mixing depths, which in turn increase average mixed layer phytoplankton light exposure and can hamper vertical nutrient exchange (Behrenfeld et al. 2005; Siegel et al. 2005). Decreased nutrient availability suppresses phytoplankton cellular chlorophyll levels and can diminish phytoplankton biomass. Likewise, acclimation to enhanced mixed layer light exposure entails reductions in cellular chlorophyll. Changes in seasonal surface mixing cycles can also influence chlorophyll levels by altering predator–prey interactions and thereby phytoplankton biomass and species composition. Thus, it is the correlation between SST and the summed expression of these direct nutrient, light, and ecosystem effects that gives rise to inverse chlorophyll–SST relationships. The relative importance of these controlling factors, however, varies over space and time (e.g., Behrenfeld et al. 2008b) and is expressed through variations in the slope of the chlorophyll–SST relationship.

Conclusions of the 2008 analysis are that 1) continuation of the satellite-based climate record for

global chlorophyll anomalies was possible, despite prolonged 2008 gaps in SeaWiFS data, because of a substantial and continuous overlap period between SeaWiFS and MODIS–*Aqua* observations; 2) the rise in chlorophyll for the stratified oceans between 2007 and 2008 corresponds with an ENSO shift toward La Niña conditions; 3) net inverse relationships between anomalies in chlorophyll and SST for the

merged data are consistent with SeaWiFS-only trends since 1997; 4) intersensor biases in ocean products, while not preventing extension of anomaly trends, do have a significant impact on quantitative assessments of global chlorophyll concentrations and NPP; and 5) continuity of satellite ocean color observations is essential for understanding global ocean biosphere changes and feedbacks (Siegel et al. 2008).

References

- Ando, K., and M. J. McPhaden, 1997: Variability of surface layer hydrography in the tropical Pacific Ocean, *J. Geophys. Res.*, **102**, 23064–23078.
- Arguez, A., and co-authors. 2007: State of the climate in 2006. *Bull. Amer. Meteor. Soc.*, **88**, Suppl., S8 – S132.
- Baehr, J., H. Haak, S. Alderson, S. A. Cunningham, J. H. Jungclaus, J. Marotzke, 2007, Timely detection of changes in the meridional overturning circulation at 26°N in the Atlantic, *J. Climate*, **20** (23), 5827-5841. doi: 10.1175/2007JCLI1686.1.
- Baehr, J., K. Keller, J. Marotzke, 2008. Detecting potential changes in the meridional overturning circulation at 26°N in the Atlantic. *Climate Change*, 91 (1-2), 11-27, doi: 10.1007/s10584-006-9153-z.
- Baringer, M. O. and J. Larsen, 2001 Sixteen Years of Florida Current Transport at 27°N. *Geophysical Research Letters*, **28**, 16, 3179-3182.
- Baringer, M. O'Neil, and R. Molinari 1999. Atlantic Ocean baroclinic heat flux at 24 to 26°N. *Geophysical Research Letters*, **26**, 3, 353-356.
- Beal, L. M., J. M. Hummon, E. Williams, O. Brown, W. Baringer, and E. Kearns, 2008, Five Years of Florida Current Structure and Transport from the Royal Caribbean Cruise ship Explorer of the Seas, *J. Geophys. Res.*, doi:10.1029/2007JC004154.
- Behrenfeld, M. J., Boss, E., Siegel, D.A., Shea, D.M., 2005: Carbon-based ocean productivity and phytoplankton physiology from space. *Global Biogeochem. Cycles*, **19**, GB1006, doi:10.1029/2004GB002299.
- Behrenfeld, M. J., Falkowski, P. G., 1997: Photosynthetic rates derived from satellite-based chlorophyll concentration. *Limnol. Oceanogr.*, **42**, 1-20.
- Behrenfeld, M. J., Halsey, K.H., Milligan, A. J., 2008b: Evolved Physiological Responses of Phytoplankton to their Integrated Growth Environment. *Phil. Trans. Royal Soc. B* **363**, doi:10.1098/rstb.2008.0019.
- Behrenfeld, M. J., O'Malley, R.T. Siegel, D. A., McClain, C. R., Sarmiento, J. L., Feldman, G. C., Milligan, A. J., Falkowski, P. G., Letelier R. M., Boss, E. S., 2006: Climate-driven trends in contemporary ocean productivity. *Nature*, **444**, 752-755.
- Bellucci, A., S. Gualdi, E. Scoccimarro, A. Navarra, 2008, NAO-ocean circulation interactions in a coupled general circulation model. *Climate Dyn.*, **31** (7-8), 759-777, doi:10.1007/s00382-008-0408-4.
- Beránger, K., L. Siefriid, B. Barnier, E. Garnier, and H. Roquet, 1999: Evaluation of operational ECMWF surface freshwater fluxes of oceans during 1991-1997, *J. Mar. Systems*, **22**, 13-36.
- Bigorre and Weller, 2008: Air-sea surface conditions in the Gulf Stream from in-situ observations. *Eos Trans. AGU*, 89(53), Fall Meet. Suppl., Abstract OS13B-1189.
- Bindoff, N.L., J. Willebrand, V. Artale, A. Cazenave, J.M. Gregory, S. Gulev, K. Hanawa, C. Le Quéré, S. Levitus, Y. Nojiri, C.K. Shum, L.D. Talley, A.S. Unnikrishnan, J. Antonov, N.R. Bates, T. Boyer, D. Chambers, B. Chao, J. Church, R. Curry, S. Emerson, R. Feely, H. Garcia, M. González-Davila, N. Gruber, S. Josey, T. Joyce, K. Kim, B. King, A. Koertzing, K. Lambeck, K. Laval, N. Lefevre, E. Leuliette, R. Marsh, C. Mauritzen, M. McPhaden, C. Millot, C. Milly, R. Molinari, R.S. Nerem, T. Ono, M. Pahlow, T.-H. Peng, A. Proshutinsky, B. Qiu, D. Quadfasel, S. Rahmstorf, S. Rintoul, M. Rixen, P. Rizzoli, C. Sabine, D. Sahagian, F. Schott, Y. Song, D. Stammer, T. Suga, C. Sweeney, M. Tamisiea, M. Tsimplis, R. Wanninkhof, J. Willis, A.P.S.

- Wong, P. Woodworth, I. Yashayaev, and I. Yasuda, 2007: Chapter 5—Observations: Oceanic climate change and sea level. In *Climate Change 2007: The Physical Science Basis. Contribution of Working Group I to the Fourth Assessment Report of the Intergovernmental Panel on Climate Change*, Solomon S., D. Qin, M. Manning, Z. Chen, M. Marquis, K.B. Averyt, M. Tignor, and H.L. Miller (eds.), Cambridge University Press, Cambridge, United Kingdom and New York, NY, U.S.A., 385–428.
- Boning, C. W., A. Dispert, M. Visbeck, S. R. Rintoul, and F. U. Schwarzkopf, 2008, The response of Antarctic Circumpolar Current to recent climate change, *Nature Geoscience*, **1**, 864-869.
- Bonjean, F., and G. Lagerloef, 2002: Diagnostic Model and Analysis of the Surface Currents in the Tropical Pacific Ocean. *J. Phys. Oceanogr.*, **32**, 2938–2954.
- Boyer, T. P., C. Stephens, J. I. Antonov, M. E. Conkright, R. A. Locarnini, T. D. O'Brien, and H. E. Garcia, 2002: *World Ocean Atlas 2001, Volume 2: Salinity*, S. Levitus, Ed., NOAA Atlas NESDIS 50, U. S. Government Printing Office, Wash., D. C., 165 pp., CD-ROMs.
- Brennan, C. E. R. J. Matear, K. Keller, 2008, Measuring oxygen concentrations to improve the detection capabilities of an ocean circulation observation array. *J. Geophys. Res.*, **113** (C2), doi:10.1029/2007JC004113.
- Bretherton, F. P., R. E. Davis, and C. Fandry, 1976 : A technique for objective analysis and design of oceanographic instruments applied to MODE-73, *Deep-Sea Res.*, **23**, 559-582.
- Bryden, H. L., H. R. Longworth and S. A. Cunningham, 2005: Slowing of the Atlantic meridional overturning circulation at 25°N. *Nature*, **438**, 655-657.
- Carlson, A. E. D. W. Oppo, R. E. Came, A. N. LeGrande, L. D. Keigwin, W. B. Curry, 2008, Subtropical Atlantic salinity variability and Atlantic meridional circulation during the last deglaciation, *Geology*, **36** (12), 991-994, doi:10.1130/G25080A.1.
- Cunninghman, S. A., T. Kanzow, D. Rayner, M. O. Baringer, W. E. Johns, J. Marotzke, H. R. Longworth, E. M. Grant, J. J-M. Hirschi, L. M. Beal, C. S. Meinen and H. L. Bryden, 2007. Temporal Variability of the Atlantic Meridional Overturning Circulation at 26.5°N. *Science*, 17 August 2007 317: 935-938 [DOI: 10.1126/science.1141304].
- Curry, R. G., and M. S. McCartney, 2001: Ocean gyre circulation changes associated with the North Atlantic oscillation. *J. Phys. Oceanogr.*, **31**, 3374 – 3400.
- Domingues, C. M., J. A. Church, N. J. White, P. J. Gleckler, S. E. Wijffels, P. M. Barker and J. R. Dunn, 2008: Improved estimates of upper-ocean warming and multi-decadal sea-level rise, *Nature*, **453**, 1090 – 1093, doi:10.1038/nature07080.
- Doney, S.C., V.J. Fabry, R.A. Feely, and J.A. Kleypas, 2009: Ocean acidification: The other CO₂ problem. *Annu. Rev. Mar. Sci.*, **1**, 169–192. doi: 10.1146/annurev.marine.010908.163834.
- Fabry, V.J., Seibel, B.A., Feely, R.A., & Orr, J.C., 2008: Impacts of ocean acidification on marine fauna and ecosystem processes. *ICES J. Mar. Sci.* **65**, 414–432.
- Fairall, C. W., E. F. Bradley, J. E. Hare, A. A. Grachev, and J. B. Edson, 2003: Bulk parameterization on air–sea fluxes: Updates and verification for the COARE algorithm. *J. Clim.*, **16**, 571–591.
- Feely, R. A., J. Boutin, C. E. Cosca, Y. Dandonneau, J. Etcheto, H. Y. Inoue, M. Ishii, C. L. Quere, D. J. Mackey, M. McPhaden, N. Metzl, A. Poisson, and R. Wanninkhof, 2002: Seasonal and interannual variability of CO₂ in the equatorial Pacific, *Deep Sea Res. II*, **49**(13-14), 2443-2469.
- Feely, R. A., T. Takahashi, R. Wanninkhof, M. J. McPhaden, C. E. Cosca, and S. C. Sutherland, 2006: Decadal variability of the air-sea CO₂ fluxes in the equatorial Pacific Ocean. *J. Geophys. Res.*,

- Feely, R.A., C.L. Sabine, J. M. Hernandez-Ayon, D. Ianson, B. Hales, 2008: Evidence for Upwelling of Corrosive "Acidified" Water onto the Continental Shelf. *Science* **320**, 1490–1492.
- Feely, R.A., Sabine, C.L., Lee, K., Berelson, W., Kleypas, J., Fabry, V.J., & Millero, F.J., 2004: Impact of anthropogenic CO₂ on the CaCO₃ system in the oceans. *Science* **305**, 362–366.
- Franz, B. A., Bailey, S. W., Werdell, P. J., McClain, C. R., 2007: Sensor-independent approach to the vicarious calibration of satellite ocean color radiometry. *Appl. Opt.* **46**, 5068-5082.
- Fukasawa, M., H. Freeland, R. Perkin, T. Watanabe, H. Uchida, and A. Nishina, 2004: Bottom water warming in the North Pacific Ocean. *Nature*, **427**, 825–827, doi:10.1038/nature02337.
- Ganachaud, A., and C. Wunsch, 2003: Large-Scale Ocean Heat and Freshwater Transports during the World Ocean Circulation Experiment. *Journal of Climate*, **16** (4), 696-705.
- Goni, G. and I. Wainer, 2001: Investigation of the Brazil Current Front Dynamics from Altimeter Data. *J. Geophys. Res.*, **36**, 31117—31128.
- Goni, G., S. Kamholz, S. Garzoli and D. Olson, 1996: Dynamics of the Brazil-Malvinas Confluence Based on Inverted Echo Sounders and Altimetry, *J. Geophys. Res.*, **101**, 16273-16289.
- Gregg, W. W., Casey, N. W., McClain, C. R., 2005: Recent trends in global ocean chlorophyll. *Geophys. Res. Lett.*, **32**, L03606, doi:10.1029/2004GL021808.
- Gruber, N., Gloor, M., Mikaloff Fletcher, S. E., Doney, S. C., Dutkiewicz, S., Follows, M., Gerber, M., Jacobson, A. R., Joos, F., Lindsay, K., Menemenlis, D., Mouchet, A., Müller, S. A., Sarmiento, J. L. and T. Takahashi, 2009: Oceanic sources, sinks, and transport of atmospheric CO₂. *Global Biogeochem. Cycles*. **23**, doi:10.1029/2008GB003349.
- Haine, T. W. N., and S. L. Gray, 2001: Quantifying mesoscale variability in ocean transient tracer fields, *J. Geophys. Res. - Oceans*, **106**, 13861-13878.
- Hall-Spencer, J.M., Rodolfo-Metalpa, R., Martin, S., Ransome, E., Fine, M., Turner, S.M., Rowley, S.J., Tedesco, D., & Buia, M.-C., 2008. Volcanic carbon dioxide vents show ecosystem effects of ocean acidification. *Nature* **454**, 96–99.
- Hansen, J., L. Nazarenko, R. Ruedy, M. Sato, J. Willis, A. Del Genio, D. Koch, A. Lacis, K. Lo, S. Menon, T. Novakov, J. Perlwitz, G. Russell, G. A. Schmidt, and N. Tausnev, 2005: Earth's energy imbalance: Confirmation and implications. *Science*, **308**, 1431 – 1435.
- Hátún, H. A. B. Sandø, H. Drange, B. Hansen, and H. Valdimarsson, 2005: Influence of the Atlantic subpolar gyre on the thermohaline circulation. *Science*, **309**, 1841-1844, doi:10.1126/science.11147777.
- Hawkins, E., R. Sutton, 2007, Variability of the Atlantic thermohaline circulation described by three-dimensional empirical orthogonal functions. *Climate Dyn.*, **29**, 745-762, doi:10.1007/s00382-007-0263-8.
- Held, I. M., and B. J. Soden, 2006: Robust response of the hydrological cycle to global warming. *J. Climate*, **19**, 5686-5699.
- Helm, K. P., N. L. Bindoff, and J. A. Church, 2009: Global hydrological-cycle changes inferred from observed ocean salinity, *Nature Geosciences*, submitted.
- Hurrell, J.W., 1995: Decadal Trends in the North Atlantic Oscillation: Regional Temperatures and Precipitation. *Science*, **269**, 676-679.
- Hutchins, D. A., Fe, F.-X., Zhang, Y, Warner, M.E., Feng, Y., Portune, K., Bernhardt, P.W., & Mulholland,

- M.R., 2007: CO₂ control of *Trichodesmium* N₂ fixation, photosynthesis, growth rates, and elemental ratios: implications for past, present, and future ocean biogeochemistry. *Limnol. Oceanog.* **52**, 1293–1304.
- Jacobs, S. S., C. F. Giulivi, and P. A. Mele, 2002: Freshening of the Ross Sea during the late 20th Century. *Science*, **297**, 386–389.
- Jacobson, A. R., S. E. Mikaloff Fletcher, N. Gruber, J. S. Sarmineto, and M. Gloor, 2007: A joint atmosphere-ocean inversion for surface fluxes of carbon dioxide: 1. Methods and global-scale fluxes. *Global Biogeochem cycles*, **21**, doi:10.1029/2005GB002556.
- Johns, W. E., L. M. Beal, M. O. Baringer, J. R. Molina, S. A. Cunningham, T. Kanzow, and D. Rayner, 2008. Variability of shallow and deep western boundary currents off the Bahamas during 2004-2005: Results from the 26°N RAPID-MOC array. *Journal of Physical Oceanography*, **38**, 605-623 [DOI: 10.1175/2007JP03791.1].
- Johnson, G. C. 2008: Quantifying Antarctic Bottom Water and North Atlantic Deep Water Volumes. *J. Geophys. Res.*, **113**, C05027, doi:10.1029/2007JC004477.
- Johnson, G. C. and S. C. Doney, 2006: Recent western South Atlantic bottom water warming. *Geophys. Res. Lett.*, **33**, L14614, doi:10.1029/2006GL026769.
- Johnson, G. C., S. G. Purkey, and J. L. Bullister, 2008: Warming and freshening in the abyssal southeastern Indian Ocean. *J. Climate*, **21**, 5351-5363, doi:10.1175/2008JCLI2384.1.
- Johnson, G. C., S. G. Purkey, and J. M. Toole. 2008b: Reduced Antarctic meridional overturning circulation reaches the North Atlantic Ocean. *Geophys. Res. Lett.*, **35**, L22601, doi:10.1029/2008GL035619.
- Johnson, G. C., S. Mecking, B. M. Sloyan, and S. E. Wijffels, 2007: Recent bottom water warming in the Pacific Ocean. *J. Climate*, **20**, 5365-5375, doi:10.1175/2007JCLI1879.1.
- Kanzow, T, S. A. Cunningham, D. Rayner, J. J-M. Hirschi, W.E. Johns, M. O. Baringer, H. L. Bryden, L. M. Beal, C. S. Meinen, J. Marotzke, 2007. Observed flow compensation associated with the meridional overturning circulation near 26.5°N in the Atlantic. *Science*, 17 August 2007, **317**: 938-941 [DOI: 10.1126/science.1141293].
- Kanzow, T. H. Johnson, D. Marshall, S. A. Cunningham, J. J-M. Hirschi, A. Mujahid, H. L. Bryden, W. E. Johns, 2009, Basin-wide integrated volume transports in an eddy-filled ocean. Submitted to *J. Phys. Ocean.*
- Kanzow, T., J. J-M. Hirschi, C. Meinen, D. Rayner, S. A. Cunningham, J. Marotzke, W. E. Johns, H. L. Bryden, L. Beal and M. O. Baringer, 2008a. A prototype system for observing the Atlantic Meridional Overturning Circulation – scientific basis, measurement and risk mitigation strategies, and first results. *Journal of Operational Oceanography*, **1**, 1, 19-28.
- Kanzow, T., U. Send, M. McCartney, 2008b, On the variability of the deep meridional transports in the tropical North Atlantic. *Deep-Sea Res.*, **55** (12), 1601-1623, doi: 10.1016/j.dsr.2008.07.011.
- Kawano T., M. Fukasawa, S. Kouketsu, H. Uchida, T. Doi, I. Kaneko, M. Aoyama, and W. Schneider, 2006b: Bottom water warming along the pathway of Lower Circumpolar Deep Water in the Pacific Ocean. *Geophys. Res. Lett.*, **33**, L23613, doi:10.1029/2006GL027933.
- Kleypas, J.A., Feely, R.A., Fabry, V.J., Langdon, C., Sabine, C.L., & Robbins, L.L., 2006: Impacts of Ocean Acidification on Coral Reefs and Other Marine Calcifiers: A Guide for Future Research, report of a workshop held 18–20 April 2005, St. Petersburg, FL, sponsored by NSF, NOAA, and the U.S. Geological Survey, 88 pp.

- Kohl, A, and D. Stammer, 2008, Variability of the meridional overturning in the North Atlantic from the 50-year GECCO state estimation, *J. Phys. Oceano.*, **38** (9), 1913-1930, doi:10.1175/2008JPO3775.1
- Kouketsu, S., M. Fukasawa, I. Kaneko, T. Kawano, H. Uchida, T. Doi, M. Aoyama, and K. Murakami, 2009: Changes in water properties and transports along 24°N in the North Pacific between 1985 and 2005, *J. Geophys. Res.*, **114**, C01008, doi:10.1029/2008JC004778.
- Kwiatkowska, E. J., Franz, B.A., Meister, G., McClain, C. R., Xiong, X., 2008: Cross calibration of ocean-color bands from Moderate Resolution Imaging Spectroradiometer on Terra platform. *Appl. Opt.*, **47**, 6796-6810.
- Le Quéré, C., C. Röedenbeck, E. T. Buitenhuis, T. J. Conway, R. Langenfelds, A. Gomez, C. Labuschagne, M. Ramonet, T. Nakazawa, N. Metzl, and N. Gillett, 2007: Saturation of the Southern ocean CO₂ sink due to recent climate change, *Science*, DOI:10.1126/science.1136188.
- LeBel, D. A., W. M. Smethie, M. Rhein, D. Kieke, R. A. Fine, J. L. Bullister, D. H. Min, W. Roether, R. F. Weiss, C. Andrie, D. Smythe-Wright, E. P. Jones, 2008, The formation rate of North Atlantic Deep Water and Eighteen Degree Water calculated from CFC-11 inventories observed during WOCE. *Deep-Sea Res.*, **55** (8), 891-910, doi:10.1016/j.dsr.2008.03.009.
- Lee, K., R. Wanninkhof, T. Takahashi, S. Doney, and R. A. Feely, 1998: Low interannual variability in recent oceanic uptake of atmospheric carbon dioxide, *Nature*, 396, 155-159.
- Leuliette, E., and L. Miller, 2009: Closing the Sea Level Rise Budget with Altimetry, Argo, and GRACE, *Geophys. Res. Lett.*, doi:10.1029/2008GL036010, in press.
- Levinson, D. H., J. H. Lawrimore, and co-authors, 2008: State of the climate in 2007. *Bull. Amer. Meteor. Soc.*, **89**, Suppl., S1 – S179.
- Levitus, S., J. I. Antonov, and T. P. Boyer, 2005: Warming of the World Ocean, 1955–2003. *Geophys. Res. Lett.*, **32**, L02604, doi:10.1029/2004GL021592.
- Levitus, S., J. I. Antonov, T. P. Boyer, R. A. Locarnini, H. E. Garcia, and A. V. Mishonov, 2009: Global Ocean Heat Content 1955–2007 in light of recently revealed instrumentation problems. *Geophys. Res. Lett.*, accepted.
- Lohmann, G. H. Haak, J. H. Jungclaus, 2008, Estimating trends of Atlantic meridional overturning circulation from long-term hydrographic data and model simulations. *Ocean Dyn.*, **58** (2), 127-138, doi:10.1007/s10236-008-0136-7.
- Lohmann, K., H. Drange, M. Bentsen, 2009, Response of the North Atlantic subpolar gyre to persistent North Atlantic oscillation like forcing. *Climate Dyn.*, **32** (2-3), 273-285, doi:10.1007/s00382-008-0467-6.
- Longworth, H. R., H. L. Bryden, M. O. Baringer, 2008. Long-term changes in Atlantic meridional baroclinic transport at 26.5°N from boundary dynamic height observations. *Journal of Physical Oceanography*, submitted.
- Lovenduski, N. S., N. Gruber, S. C. Doney, and I. D. Lima, 2007: Enhanced CO₂ outgassing in the Southern Ocean from a positive phase of the Southern Annular Mode, *Global Biogeochem cycles*, 21, GB2026, doi:10.1029/2006GB002900.
- Lumpkin, R. and K. Speer, 2007: Global Ocean meridional overturning. *J. Phys. Oceanogr.*, **37**, 2550–2562.
- Lumpkin, R. and M. Pazos, 2007: Measuring surface currents with Surface Velocity Program drifters: the instrument, its data, and some recent results. Chapter 2 of "Lagrangian

Analysis and Prediction of Coastal and Ocean Dynamics", ed. A. Griffa, A. D. Kirwan, A. Mariano, T. Özgökmen and T. Rossby, Cambridge University Press.

- Lumpkin, R., K.G. Speer and K.P. Koltermann, 2008: Transport across 48°N in the Atlantic Ocean. *Journal of Physical Oceanography*, **38** (4), 733-752, doi: 10.1175/2007JPO3636.1.
- Lüthi, D., Le Floch, M., Bereiter, B., Blunier, T., Barnola, J.-M., Siegenthaler, U., Raynaud, D., Jouzel, J., Fisher, H., Kawamura, K., & Stocker, T.F., 2008: High-resolution carbon dioxide concentration record 650,000–800,000 years before present. *Nature* **435**, 379–382.
- Lyman, J. M. and G. C. Johnson, 2008: Estimating global upper ocean heat content despite irregular sampling. *J. Climate*, **21**, 5629 – 5641, doi:10.1175/2008JCLI2259.1.
- M.J. Behrenfeld, D.A. Siegel, R.T. O'Malley. 2008a. Global ocean phytoplankton and productivity. In: [J.M. Levy, ed.] *State of the Climate in 2007*. **Bull. Amer. Meteor. Soc.** July 2008. pp. S56-S61.
- MacKinnon, J. A., T. M. S. Johnson, R. Pinkel, 2008, Strong transport and mixing of deep water through the Southwest Indian Ridge. *Nature Geoscience*, **1**, 755-758, doi:10.1038/ngeo340.
- Maclay, K.S., M. DeMaria and T.H. Vonder Haar, 2008: Tropical cyclone inner core kinetic energy evolution. *Mon. Wea. Rev.*, **136**, 4882-4898.
- Maes, C., K. Ando, T. Delcroix, W. S. Kessler, M. J. McPhaden, and D. Roemmich, 2006: Observed correlation of surface salinity, temperature and barrier layer at the eastern edge of the western Pacific warm pool. *Geophys. Res. Lett.*, **33**, L06601, doi:10.1029/2005GL024772
- Mainelli, M., M. DeMaria, L. K. Shay, and G. Goni, 2008: Application of oceanic heat content estimation to operational forecasting of recent Atlantic category 5 hurricanes, *Weather and Forecasting*, **32**, 3 – 16.
- Mantua, N. J. and S. R. Hare, Y. Zhang, J. M. Wallace, and R. C. Francis, 1997: A Pacific interdecadal climate oscillation with impacts on salmon production. *Bull. Amer. Meteor. Soc.*, **78**, 1069 – 1079.
- Mantua, N.J. and S.R. Hare, Y. Zhang, J.M. Wallace, and R.C. Francis 1997: A Pacific interdecadal climate oscillation with impacts on salmon production. *Bull. Amer. Meteorol. Soc.*, **78**, 1069-1079.
- McClain, C. R., 2009: A Decade of Satellite Ocean Color Observation. *Annual Review of Marine Science*, **1**, 19-42.
- McDonagh, E. L., H. L. Bruden, B. A. King, R. J. Saunders, 2008: The circulation of the Indian Ocean at 32°S. *Prog. Oceanogr.*, **79**, 20-36, doi: 10.1016/j.pocean.2008.07.001.
- Meinen, C. S., M. O. Baringer, and R. F. Garcia, 2009, Florida Current Transport Variability: An Analysis of Annual and Longer-Periods. *J. Geophys. Res.*, (submitted).
- Molinari, R. L., E. Johns and J. F. Festa, 1990, The annual cycle of meridional heat-flux in the Atlantic Ocean at 26.5°N. *J. Phys. Oceano.*, **20**, 3, 476-482, doi:10.1175/1520-485(1990)020<0476:TACOMH>2.0.CO;2.
- Mooers, Christopher N. K., Christopher S. Meinen, Molly O. Baringer, Inkweon Bang, Robert Rhodes, Charlie N. Barron, and Frank Bub, 2005. Florida Current Response to Cold Front Passages: Comparison of NOAA Cable and Navy Model Volume Transports, *EOS*, **86**(29), pgs 269, 272-273.
- Nerem, R. S., et al., On the recent slowing of sea level rise and its relation to ENSO, in preparation, 2009.

- Niiler, P.P., R. E. Davis, et al., 1987: Water-following characteristics of a mixed layer drifter. *Deep-Sea Res.*, **34** (11), 1867-1881.
- Olsen, S. M., B. Hansen, D. Quadfasel, S. Osterhus, 2008, Observed and modelled stability of overflow across the Greenland-Scotland ridge, *Nature*, **455** (7212), 519-U35, doi:10.1038/nature07302
- Orsi, A. H., G. C. Johnson, and J. L. Bullister. 1999: Circulation, mixing, and production of Antarctic Bottom Water. *Prog. Oceanogr.*, **43**, 55-109, doi:10.1016/S0079-6611(99)00004-X.
- Palacios, S. L. and Zimmerman, R. C., 2007: Response of eelgrass *Zostera marina* to CO₂ enrichment: possible impacts of climate change and potential for remediation of coastal habitats. *Marine Ecology Progress Series*, **344**, 1-13.
- Park, G.-H., K. Lee, R. Wanninkhof, and R. A. Feely, 2006: Empirical temperature-based estimates of variability in the oceanic uptake of CO₂ over the past 2 decades, *J Geophys. Res.*, **111**, doi:10.1029/2005JC003090.
- Peacock, S., M. Maltrud, and R. Bleck, 2005: Putting models to the data test: a case study using Indian Ocean CFC-11 data, *Ocean Modelling*, **9**, 1-22.
- Peng, G., Z. Garraffo, G. R. Halliwell, O.-M. Smedstad, C. S. Meinen, V. Kourafalou, and P. Hogan, 2009, Temporal Variability of the Florida Current Transport at 27°N, in "Ocean Circulation and El Nino: The New Research", ed. F. Columbus, NOVA Science Publishers, Hauppauge, NY, (in press).
- Reynolds, R. W., N. A. Rayner, T. M. Smith, D. C. Stokes and W. Wang, 2002: An improved in situ and satellite SST analysis for climate. *J. Climate*, **15**, 1609-1625.
- Reynolds, RW and Y. Xue, 2008: Sea Surface Temperatures in 2007. In *State of the Climate in 2007*, D. H. Levinson and J. H. Lawrimore (eds.). *Bull. Am. Meteorol. Soc.*, **89**(7), S37-S39.
- Rintoul, S. R., 2007: Rapid freshening of Antarctic Bottom Water formed in the Indian and Pacific Oceans. *Geophys. Res. Lett.*, **34**, L06606, doi:10.1029/2006028550.
- Roemmich, D., S. Riser, R. Davis, and Y. Desaubies, 2004: Autonomous profiling floats: Workhorse for broadscale ocean observations. *J. Mar. Technol. Soc.*, **38**, 31 - 39.
- Sabine, C.L., Feely, R. A., Gruber, N., Key, R.M., Lee, K., Bullister, J.L., Wanninkhof, R., Wong, C.S., Wallace, D.W.R., Tilbrook, B., Millero, F.J., Peng, T.-H., Kozyr, A, Ono, T., & Rios, A.F., 2004: The oceanic sink for anthropogenic CO₂. *Science* **305**, 367-371.
- Sabine, C.L., R.A. Feely, R. Wanninkhof, and T. Takahashi, 2008: The global ocean carbon cycle. In *State of the Climate in 2007*, D. H. Levinson and J. H. Lawrimore (eds.). *Bull. Am. Meteorol. Soc.*, **89**(7), S52-S56.
- Salisbury, J., Green, M., Hunt, C. & Cambell, J., 2008. Coastal acidification by rivers: a new threat to shellfish. *Eos Trans. AGU*, **89** (50), 513.
- Schmid, C., 2005: Impact of combining temperature profiles from different instruments on an analysis of mixed layer properties, *J. Atmos. Oceanic Technol.*, **22**, 1571 -1587.
- Schott, F. A., J. Fischer, M. Dengler, R. Zantopp, 2006, Variability of the Deep Western Boundary Current east of Grand Banks. *Geophys. Res. Lett.*, **33** (21), doi:10.1029/2006GL026563.
- Schuster, U., and A. J. Watson, 2007: A variable and decreasing sink for atmospheric CO₂ in the North Atlantic, *J Geophys. Res.*, **112**, doi:10.1029/2006JC003941.
- Shay, L. K., G. J. Goni, and P. G. Black, 2000: Effects of a warm oceanic feature on Hurricane Opal. *Mon. Wea. Rev.*, **128**: 1366-1383.

- Siegel, D. A., Yoder, J. A., McClain, C. R., 2008: Thoughts about the future of satellite ocean color observations, OCB Newsletter, Oct. 2008, pages 7-8, Ocean Carbon and Biogeochemistry Project Office, Woods Hole, MA (http://www.us-cb.org/publications/OCB_NEWS_OCT08.pdf).
- Siegel, D.A., Maritorena, S., Nelson, N.B., Behrenfeld, M.J., 2005: Independence and interdependences among global ocean color properties: Reassessing the bio-optical assumption. *J. Geophys. Res.* **110**, C07011, doi:10.1029/2004JC002527
- Smith, T.M., R. W. Reynolds, T. C. Peterson, and J. Lawrimore, 2008: Improvements to NOAA's historical merged land-ocean surface temperature analysis (1880-2006). *J. Climate*, **21**, 2283-2296.
- Stammer, D., 1998: On Eddy Characteristics, Eddy Transports, and Mean Flow Properties. *J. Phys. Oceanogr.*, **28**, 727-739.
- Takahashi, T., S. C. Sutherland, R. Wanninkhof, C. Sweeney, R. A. Feely, D. W. Chipman, B. Hales, G. Friederich, F. Chavez, C. Sabine, A. Watson, D. C. E. Bakker, U. Schuster, N. Metzl, H. Yoshikawa-Inoue, M. Ishii, T. Midorikawa, Y. Nojiri, A. Körtzinger, T. Steinhoff, M. Hoppema, J. Olafsson, T. S. Arnarson, B. Tilbrook, T. Johannessen, A. Olsen, R. Bellerby, C. S. Wong, B. Delille, N. R. Bates, and H. J. W. deBaar, 2008: Climatological Mean and Decadal Change in Surface Ocean pCO₂, and Net Sea-air CO₂ Flux over the Global Oceans. *Deep -Sea Res. II*, 56, doi:10.1016/j.dsr2.2008.12.009. (Errata available from the lead author.)
- Talley, L. D., 2008. Freshwater transport estimates and the global overturning circulation: Shallow, deep and throughflow components, *Progress in Oceanography*, **78** (3), doi: 10.1016/j.pocean.2008.05.001.
- Tans, P.P., I.Y. Fung, and T. Takahashi, 1990: Observational constraints on the global atmospheric CO₂ budget. *Science*, **247**, 1431-1439, doi:10.1126/science.247.4949.1431.
- Thomas, H., A. E. Friederike Prowe, I. D. Lima, S. C. Doney, R. Wanninkhof, R. J. Greatbach, U. Schuster, and A. Corbiere, 2008: Changes in the North Atlantic Oscillation influence CO₂ uptake in the North Atlantic over the past two decades, *Global Biogeochem cycles*, **22**, GB4027, doi:4010.1029/2007GB003167.
- Våge, K., R. S. Pickart, V. Thierry, G. Reverdin, C. M. Lee, B. Petrie, T. A. Agnew, A. Wong, and M. H. Ribergaard, 2009: Surprising return of deep convection to the subpolar North Atlantic Ocean in winter 2007-2008. *Nature Geoscience*, **2**, 67-72, doi:10.1038/ngeo382.
- Vecchi, G. A., K. L. Swanson, and B. J. Soden, 2008: CLIMATE CHANGE: Whither Hurricane Activity? *Science*, **322**, 687 - 689, doi:10.1126/science.1164396.
- Wallace, D. W. R., 1995: *Monitoring global ocean carbon inventories*, 54 pp, Texas A&M University, College Station, TX.
- Wijffels, S. E., J. Willis, C. M. Domingues, P. Barker, N. J. White, A. Gronell, K. Ridgway, and J. A. Church, 2008: Changing expendable bathythermograph fall-rates and their impact on estimates of thermosteric sea level rise *J. Climate*, **21**, 5657-5672.
- Wijffels, S. E., R. W. Schmitt, H. L. Bryden and A. Stigebrandt, 1992: Freshwater transport by the ocean. *J. Phys. Oceanogr.*, **22**, 155-162.
- Willis, J. K., D. P. Chambers, and R. S. Nerem, 2008: Assessing the globally averaged sea level budget on seasonal and interannual timescales, *J. Geophys. Res.* **113**, C06015, doi:10.1029/2007JC004517.

- Willis, J. K., D. Roemmich, and B. Cornuelle, 2004: Interannual variability in upper ocean heat content, temperature, and thermosteric expansion on global scales. *J. Geophys. Res.*, **109**, C12036, doi: 10.1029/2003JC002260.
- Wunsch, C, 2008, , Mass and volume transport variability in an eddy-filled ocean. *Nature Geoscience*, **1** (3)165-168, doi:10.1038/ngeo126.
- Wunsch, C. and P. Heimbach, 2006, Estimated decadal changes in the North Atlantic meridional overturning circulation and heat flux 1993-2004. *J. Phys. Oceanogr.*, **36** (11), 2012-2024, doi:10.1175/JPO2957.1.
- Xue, Y., T. M. Smith, and R. W. Reynolds, 2003: Interdecadal changes of 30-yr SST normals during 1871-2000. *J. Climate*, **16**, 1601-1612.
- Yashayaev, I., and J. W. Loder, 2009, Enhanced production of Labrador Sea Water in 2008. *Geophys. Res. Lett.*, **36**, Doi:10.1029/2008GL036162.
- Yu, L., X. Jin, and R. A. Weller, 2008: Air-sea turbulent heat flux estimates at the global buoy sites. *J. Climate*. *Sub judice*.
- Yu, L., X. Jin, and R. A. Weller, 2008: Multidecade Global Flux Datasets from the Objectively Analyzed Air-sea Fluxes (OAFlux) Project: Latent and sensible heat fluxes, ocean evaporation, and related surface meteorological variables. Woods Hole Oceanographic Institution, OAFlux Project Technical Report. OA-2008-01, 64pp. Woods Hole. Massachusetts.
- Zebiak, S. E., 1989: Oceanic heat content variability and El Niño cycles. *J. Phys. Oceanogr.*, **19**, 475-486.
- Zhang, R, 2008, Coherent surface-subsurface fingerprint of the Atlantic meridional overturning circulation, *Geophys. Res. Lett.*, **35** (20), Doi:10.1029/2008GL035463.